

# Metabolites released from apoptotic cells act as tissue messengers

<https://doi.org/10.1038/s41586-020-2121-3>

Received: 29 January 2019

Accepted: 18 February 2020

Published online: 18 March 2020

 Check for updates

Christopher B. Medina<sup>1,2</sup>, Parul Mehrotra<sup>3,8</sup>, Sanja Arandjelovic<sup>1,2,8</sup>, Justin S. A. Perry<sup>1,2,8</sup>, Yizhan Guo<sup>4</sup>, Sho Morioka<sup>1,2</sup>, Brady Barron<sup>1,5</sup>, Scott F. Walk<sup>1,2</sup>, Bart Ghesquière<sup>6</sup>, Alexander S. Krupnick<sup>4,7</sup>, Ulrike Lorenz<sup>2,7</sup> & Kodi S. Ravichandran<sup>1,2,3,7</sup>✉

Caspase-dependent apoptosis accounts for approximately 90% of homeostatic cell turnover in the body<sup>1</sup>, and regulates inflammation, cell proliferation, and tissue regeneration<sup>2–4</sup>. How apoptotic cells mediate such diverse effects is not fully understood. Here we profiled the apoptotic metabolite secretome and determined its effects on the tissue neighbourhood. We show that apoptotic lymphocytes and macrophages release specific metabolites, while retaining their membrane integrity. A subset of these metabolites is also shared across different primary cells and cell lines after the induction of apoptosis by different stimuli. Mechanistically, the apoptotic metabolite secretome is not simply due to passive emptying of cellular contents and instead is a regulated process. Caspase-mediated opening of pannexin 1 channels at the plasma membrane facilitated the release of a select subset of metabolites. In addition, certain metabolic pathways continued to remain active during apoptosis, with the release of only select metabolites from a given pathway. Functionally, the apoptotic metabolite secretome induced specific gene programs in healthy neighbouring cells, including suppression of inflammation, cell proliferation, and wound healing. Furthermore, a cocktail of apoptotic metabolites reduced disease severity in mouse models of inflammatory arthritis and lung-graft rejection. These data advance the concept that apoptotic cells are not inert cells waiting for removal, but instead release metabolites as ‘good-bye’ signals to actively modulate outcomes in tissues.

Apoptosis occurs during development<sup>3</sup>, homeostatic tissue turnover, and in pathological settings<sup>1</sup>. Besides the known responses of phagocytes that engulf apoptotic cells<sup>4</sup>, the apoptotic process itself (independent of phagocytosis) can modulate physiological events, such as embryogenesis and tissue regeneration<sup>5</sup>, with pathologies arising when apoptosis is inhibited<sup>6</sup>. However, the mechanisms by which apoptotic cells themselves mediate these functions are not well understood. As apoptotic cells remain intact for a period of time, they could release soluble metabolites that diffuse within a tissue to influence neighbouring cells. Although a few soluble factors from apoptotic cells are reported as ‘find-me’ signals to attract phagocytes<sup>7</sup>, the full apoptotic secretome is not yet defined.

To profile the metabolite secretome of apoptotic cells, we used human Jurkat T cells, primary mouse thymocytes, or primary mouse bone-marrow-derived macrophages (BMDMs), all of which can undergo inducible, caspase-dependent apoptosis (caused by ultraviolet (UV)-light treatment, anti-Fas antibody crosslinking, or treatment with anthrax lethal toxin)<sup>8,9</sup> (Fig. 1a). As untargeted metabolomics require large numbers of cells, we optimized the parameters using Jurkat cells (for example, cell density, culture volume and duration after apoptosis), such that approximately 80% of the cells were apoptotic, while

maintaining cell membrane integrity (annexin V<sup>7</sup>AAAD<sup>−</sup>) (Extended Data Fig. 1a, b). Supernatants and cell pellets from apoptotic cells and live cell controls were subjected to untargeted metabolomic profiling against a library of more than 3,000 biochemical features or compounds. Supernatants of apoptotic Jurkat cells (induced by UV irradiation) showed an enrichment of 123 metabolites (Fig. 1b, Extended Data Fig. 1c, d, Supplementary Table 1), and 85 of these 123 were reciprocally reduced in the apoptotic cell pellets (Extended Data Fig. 2a–f, Supplementary Table 2).

In untargeted metabolomics of supernatants from macrophages undergoing apoptosis (induced via anthrax lethal toxin<sup>9</sup>), we detected fewer metabolites (20 versus 123 in Jurkat cells), perhaps owing to differences in cell types, modality of death and/or quantities released (below detection limits). Notably, 16 of the 20 metabolites (80%) were shared with apoptotic Jurkat cells (Fig. 1b).

For further validation and quantification, we performed targeted metabolomics and analysed 116 specific metabolites (Methods) in the supernatants from Jurkat cells and primary mouse thymocytes after Fas-crosslinking (extrinsic cue for apoptosis) (Supplementary Table 3). This targeted panel included 43 of the metabolites released from apoptotic Jurkat cells (identified above), and included a 5-kDa filtering step

<sup>1</sup>Center for Cell Clearance, University of Virginia, Charlottesville, VA, USA. <sup>2</sup>Department of Microbiology, Immunology, and Cancer Biology, University of Virginia, Charlottesville, VA, USA. <sup>3</sup>VIB/UGent Inflammation Research Centre, Biomedical Molecular Biology, Ghent University, Ghent, Belgium. <sup>4</sup>Department of Surgery, University of Virginia, Charlottesville, VA, USA. <sup>5</sup>Department of Pharmacology, University of Virginia, Charlottesville, VA, USA. <sup>6</sup>Department of Oncology and VIB, KU Leuven, Leuven, Belgium. <sup>7</sup>Carter Immunology Center, University of Virginia, Charlottesville, VA, USA. <sup>8</sup>These authors contributed equally: Parul Mehrotra, Sanja Arandjelovic, Justin Perry. <sup>✉</sup>e-mail: Ravi@virginia.edu

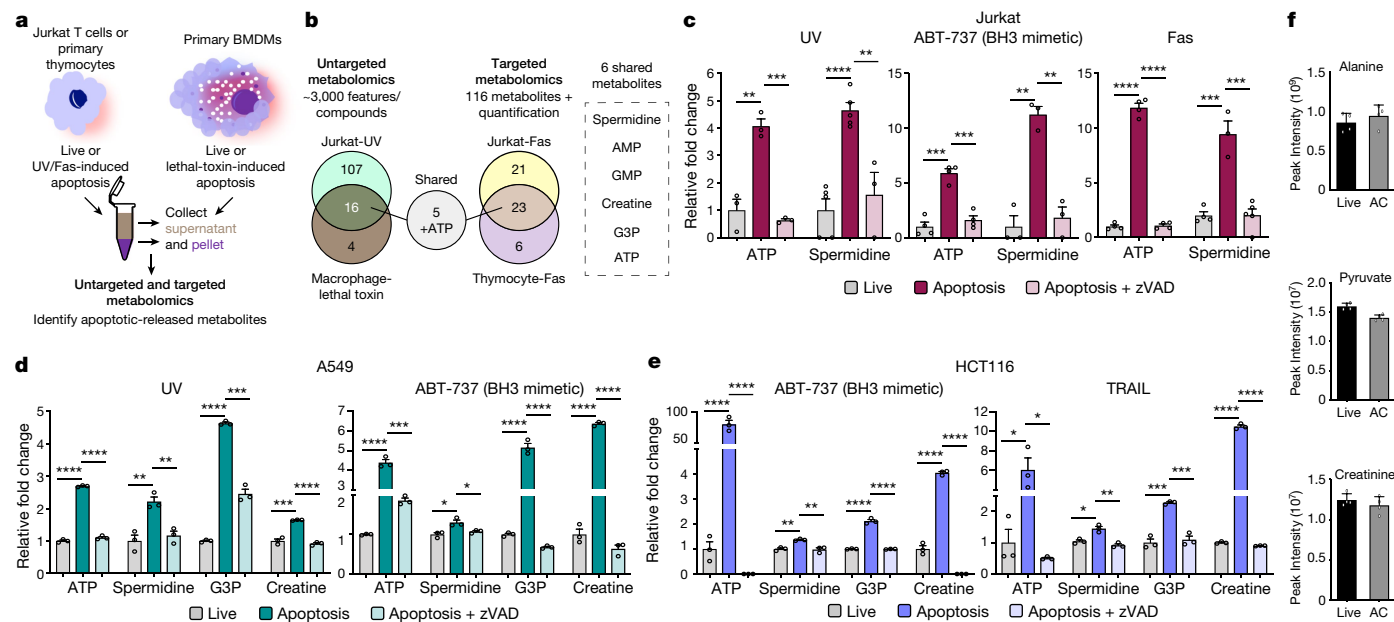


**Fig. 1 | Conserved metabolite secretome from apoptotic cells.** **a**, Schematic for assessing apoptotic metabolite secretomes. **b**, Venn diagrams illustrating the shared apoptotic metabolites identified across cell types, modalities of apoptosis induction, and the two metabolomic platforms tested, and the list of five shared metabolites plus ATP. G3P, glycerol-3-phosphate. **c–e**, Metabolite release from Jurkat T cells ( $n = 3$  for ATP–UV, spermidine–UV + zVAD, spermidine–ABT, and spermidine–Fas;  $n = 4$  for ATP–ABT, ATP–Fas and spermidine–Fas–live;  $n = 5$  for spermidine–UV–live and spermidine–

Fas + zVAD) (**c**), A549 lung epithelial cells ( $n = 3$ ) (**d**), and HCT-116 colonic epithelial cells ( $n = 3$ ) (**e**) across different apoptotic stimuli, with or without inhibition of caspase using zVAD. **f**, Several abundant metabolites such as alanine (top), pyruvate (middle) and creatinine (bottom) were not released in the Jurkat T cell supernatants ( $n = 4$ ). AC, apoptotic cell. \* $P < 0.05$ , \*\* $P < 0.01$ , \*\*\* $P < 0.001$ , \*\*\*\* $P < 0.0001$ , unpaired Student's *t*-test with Holm–Sidak method for multiple *t*-tests. Data are mean  $\pm$  s.e.m. (**c–e**) or mean  $\pm$  s.d. (for **f**).

to exclude proteins and extracellular vesicles. This targeted analysis showed an enrichment of many metabolites seen with UV-induced apoptosis (Fig. 1b). Furthermore, metabolites released from apoptotic primary thymocytes overlapped with apoptotic Jurkat cells (Fig. 1b). Comparison of metabolites enriched or released in the apoptotic supernatant of Jurkat cells, thymocytes and macrophages (after Fas-, UV- or toxin-mediated apoptosis) identified five conserved metabolites: adenosine monophosphate (AMP), guanosine 5'-monophosphate (GMP), creatine, spermidine and glycerol-3-phosphate (Fig. 1b, Extended Data Fig. 3a). ATP represents the sixth shared metabolite (via luciferase assay) (Extended Data Fig. 3b), although ATP was not profiled in the metabolomic analyses for technical reasons.

To test other cell types and apoptotic modalities, we analysed the release of four conserved metabolites via analytical kits. Jurkat cells, A549 lung epithelial cells and HCT116 colonic epithelial cells were induced to undergo death via different apoptotic cues, such as UV radiation, treatment with the BH3-mimetic ABT-737 (which directly induces permeabilization of the mitochondrial outer membrane), and/or treatment with TRAIL (the cell extrinsic pathway) (Fig. 1c–e). We could readily detect apoptosis-dependent release of the tested metabolites, and attenuation by pan-caspase inhibitor zVAD (Fig. 1c–e, Extended Data Fig. 3c). The metabolites detected were not due to simple emptying of cellular contents during apoptosis, as many metabolites at high intracellular concentrations were not released (Fig. 1f). These data reveal apoptotic cells as a natural source of many metabolites with biological functions.

During the above analyses, we noted that despite the many cellular metabolites detected in the pellet only a subset is released; furthermore, even within a known metabolic pathway, only some were released. Such selectivity could arise from specific channels that open during apoptosis to permeate certain metabolites, and/or continued metabolic activity within the dying cell influencing the secretome. To test specific channels, we focused on pannexin 1 (PANX1) channels

that are activated during apoptosis by caspase-mediated cleavage<sup>10</sup> and can conduct ions and small molecules up to 1 kDa in size across the plasma membrane. In a PANX1-dependent manner<sup>10</sup>, apoptotic cells (but not live cells) take up the nucleic acid stain TO-PRO-3 dye (671 Da), whereas 7AAD (1.27 kDa) is excluded (Extended Data Fig. 4a, b). We tested the relevance of PANX1 by genetic and pharmacological approaches. Genetically, we used Jurkat cells expressing a dominant-negative PANX1 with a mutation in the caspase cleavage site<sup>10</sup> (PANX1-DN) or primary thymocytes from PANX1-deficient mice (*Panx1*<sup>-/-</sup>)<sup>11</sup>. We also used two pharmacological inhibitors, trovafloxacin (Trovan) and spironolactone, which had previously been identified in unbiased screens<sup>11,12</sup>. Disrupting PANX1 activity per se did not affect apoptosis (Extended Data Fig. 5a–e). Untargeted metabolomics of the supernatants from apoptotic Jurkat cells (UV-induced) with and without PANX1 inhibition revealed that PANX1 contributed to release approximately 20% of the apoptotic metabolites (25 out of 123) (Fig. 2a, Extended Data Fig. 6a). The PANX1-dependent metabolites included nucleotides, nucleotide-sugars, and metabolites linked to energy metabolism and amino acid metabolism; notably, most have not previously been reported to permeate through PANX1. A similar PANX1-dependent metabolite signature was shared between Jurkat cells and thymocytes; furthermore, as not all apoptotic metabolites released were PANX1-dependent, other mechanisms of metabolite release from apoptotic cells must also exist (Extended Data Fig. 6b–e). We noted eight shared PANX1-dependent apoptotic metabolites between Jurkat cells and primary thymocytes (Fig. 2b, Extended Data Fig. 7).

To test whether the apoptotic secretome might also be influenced by the metabolic activity within the dying cell, we chose the polyamine pathway for several reasons. First, the polyamine spermidine was released in considerable quantities from apoptotic Jurkat cells, macrophages, thymocytes and epithelial cells after different modes of apoptosis induction (Fig. 2c). Second, among the two metabolites immediately upstream of spermidine, putrescine was not released,

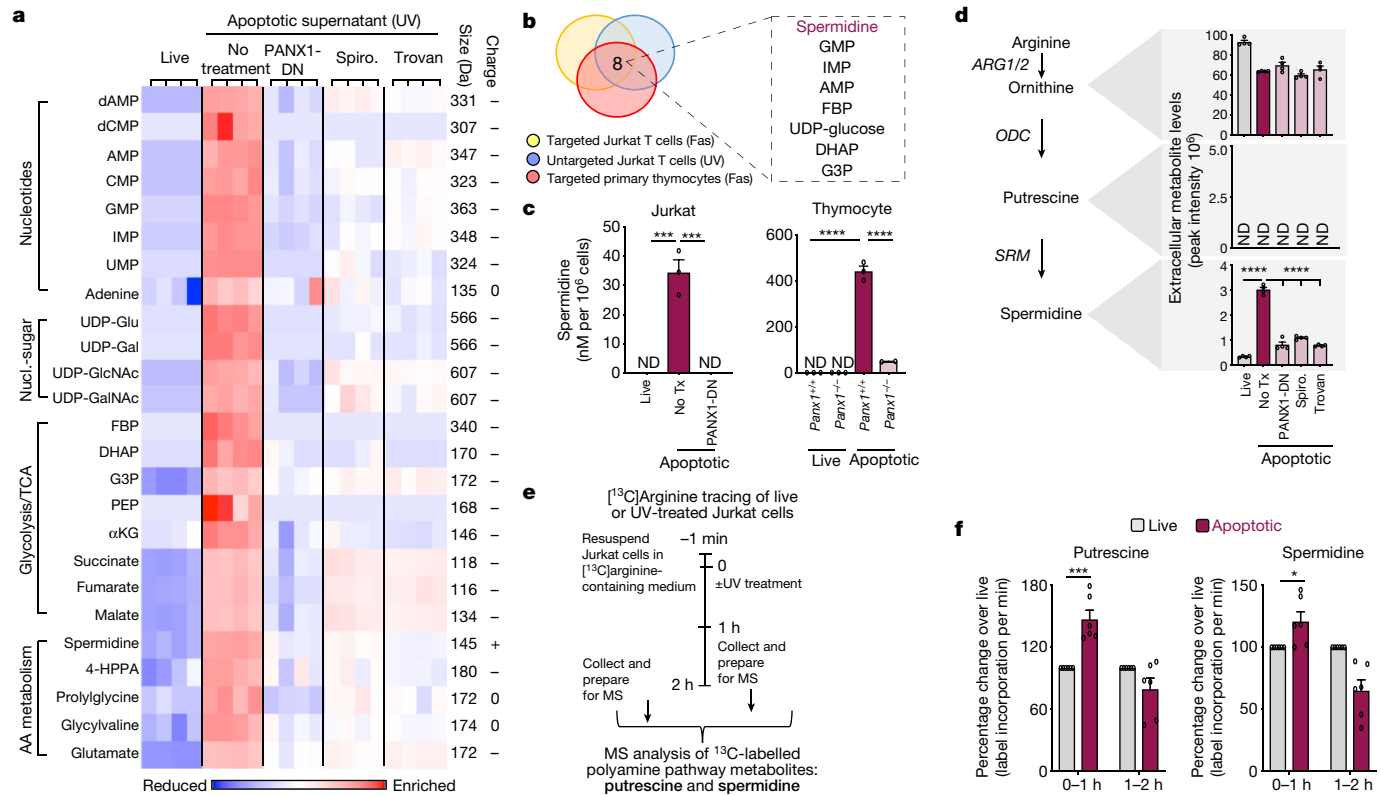


**Fig. 2 | Activation of PANX1 and continued metabolic activity of dying cells orchestrates metabolite release. a**, PANX1-dependent metabolite release. Heat map produced from untargeted metabolomics of supernatants from Jurkat T cells representing the metabolites that were statistically enriched or reduced ( $P < 0.05$ , two-sided Welch's two-sample  $t$ -test) in the apoptotic supernatants relative to live supernatants, and after inhibition of PANX1 by PANX1-DN or the PANX1 inhibitors spiroinolactone (Spiro.) or trovafloxacin (Trovan). Metabolites are grouped by pathway. Charge and relative sizes of the metabolites are also shown ( $n = 4$ ). 4-HPPA, 4-hydroxyphenylpyruvic acid;  $\alpha$ KG,  $\alpha$ -ketoglutarate; GalNAc,  $N$ -acetylgalactosamine; GlcNAc,  $N$ -acetylglucosamine; PEP, phosphoenolpyruvate. **b**, Three-way Venn diagram (left) illustrating the eight PANX1-dependent apoptotic metabolites observed (right) among the cell types and apoptotic modalities tested. ATP (not detected here) represents the ninth metabolite. **c**, Spermidine concentration per million cells in supernatants from targeted metabolomics in Jurkat cells (after 4 h Fas

crosslinking) (left) ( $n = 3$ ) or primary thymocytes with *Panx1* deletion (after 1.5 h Fas crosslinking) (right) ( $n = 3$ ).  $***P = 0.0002$ ,  $****P = 0.0001$ , one-way analysis of variance (ANOVA) with Turkey's multiple comparison test. ND, not determined; No Tx, no treatment. **d**, Left, schematic of the polyamine metabolic pathway. Right, relative amounts of ornithine (top), putrescine (middle) and spermidine (bottom) in supernatants of Jurkat T cells in live and apoptotic conditions, with or without PANX1 inhibition ( $n = 4$ ).  $****P = 0.0001$ , one-way ANOVA with Turkey's multiple comparison test. **e, f**, Active polyamine metabolic activity during apoptosis. Experimental layout for [<sup>13</sup>C]arginine labelling (**e**), and incorporation of [<sup>13</sup>C]-labelled arginine into the polyamine pathway intermediates putrescine (**f**, left) or spermidine (**f**, right) after the induction of cell death ( $n = 6$ ). MS, mass spectrometry.  $*P = 0.025$ ,  $***P = 0.0003$ , unpaired Student's  $t$ -test with Holm-Sidak method for multiple  $t$ -tests. Data are mean  $\pm$  s.e.m.

whereas ornithine was present comparably in live and apoptotic cell supernatants (Fig. 2d). Third, although exogenous supplementation of spermidine can reduce inflammation and improve longevity<sup>13</sup>, spermidine release from apoptotic cells provides the first natural or physiological extracellular source of this polyamine.

The upstream steps of spermidine generation involve arginine to ornithine to putrescine to spermidine, with each conversion regulated by specific enzymes. A recent report<sup>14</sup> has shown that although most mRNA gets degraded in apoptotic HCT-116 cells, a small fraction is retained. In our re-analysis of this mRNA dataset, the polyamine pathway enzyme transcripts were not degraded during apoptosis, including spermidine synthase (SRM) that converts putrescine to spermidine<sup>14</sup> (Extended Data Fig. 8a). We confirmed that in apoptotic Jurkat cells, the mRNA for spermidine synthase (SRM) was retained (Extended Data Fig. 8b). To address this more directly by metabolic flux labelling, we added medium containing [<sup>13</sup>C]arginine to Jurkat cells immediately before the induction of apoptosis, and traced incorporation of the label into putrescine and spermidine for the next few hours (Fig. 2e). Apoptotic cells displayed increased incorporation of the <sup>13</sup>C label into the polyamine pathway in the first hour, compared with live cells. After normalizing for total label incorporation and focusing on the carbons within the polyamine

pathway (Methods), apoptotic cells showed 40% and 25% greater incorporation of the <sup>13</sup>C label per minute into putrescine and spermidine, respectively, during the first hour (Fig. 2f). Although this dips during the second hour, it was still comparable to live cells. In addition, <sup>13</sup>C-labelled spermidine was detectable in the supernatants of apoptotic cells, and this was partially reduced by the inhibition of caspases (Extended Data Fig. 8c). Notably, despite its active generation (revealed by <sup>13</sup>C-labelling analysis), putrescine was not detected in apoptotic cell supernatants from Jurkat cells (or in the macrophage or thymocytes dataset) (Fig. 2d). Thus, apoptotic cells orchestrate the generation and release of select metabolites at least at two levels: caspase-dependent opening of specific channels (PANX1) and continued metabolic activity of certain pathways.

To test whether released metabolites derived from apoptotic cells signal to alter gene expression programs in healthy nearby cells such as phagocytes, we added supernatants from live or apoptotic Jurkat cells (same conditions as untargeted metabolomics) to phagocytic LR73 cells—a Chinese hamster ovary cell line that is useful for determining mechanisms or responses after efferocytosis<sup>15–17</sup> (Fig. 3a). RNA sequencing (RNA-seq) analysis of LR73 cells (after 4 h) indicated distinct transcriptional changes (Fig. 3b, Extended Data Fig. 9a). Pathway analysis, by curating each of the hits individually,

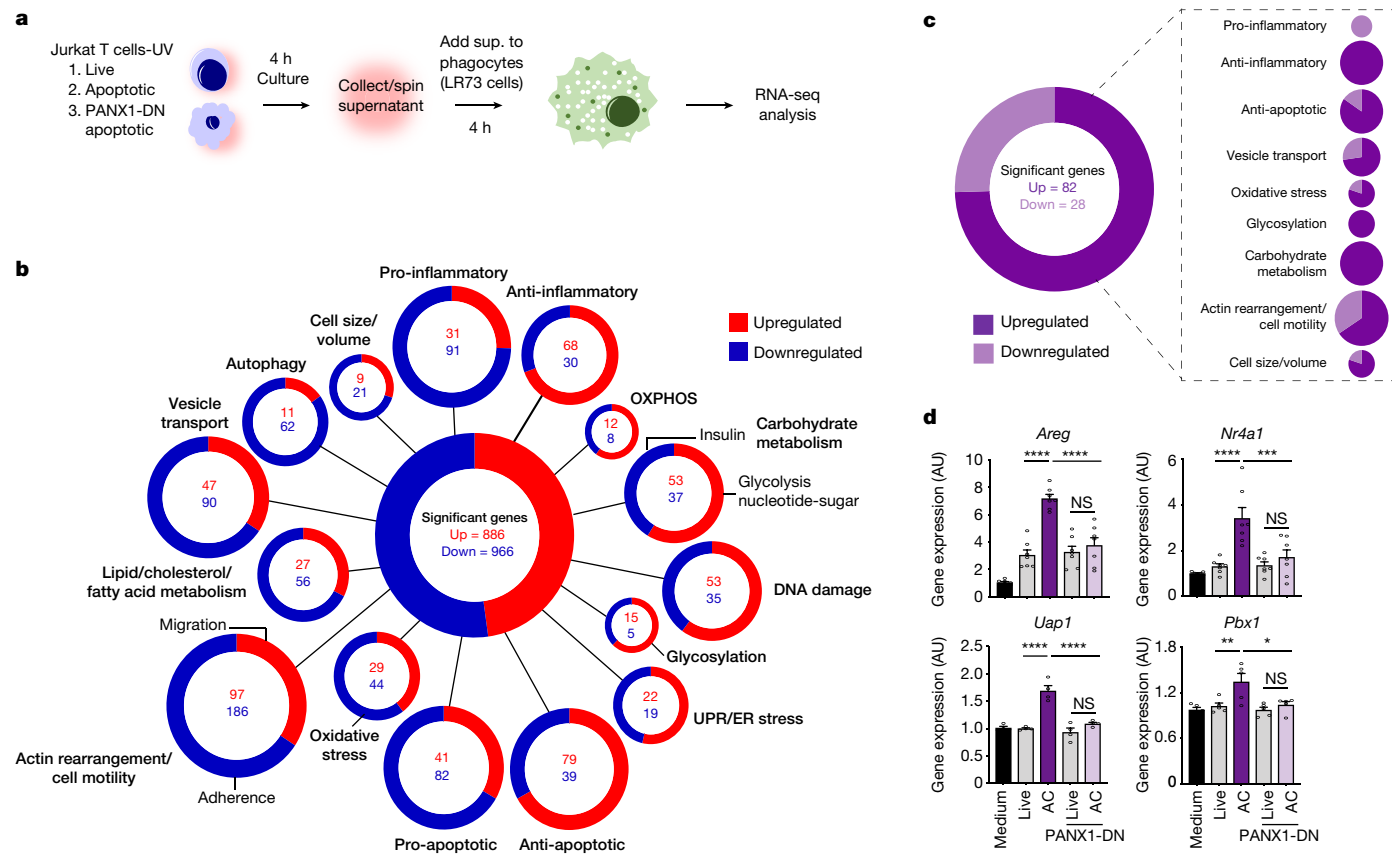


**Fig. 3 | Metabolites from apoptotic cells influence gene programs in live cells.** **a**, Schematic for assessing gene induction by apoptotic cell supernatants in LR73 cells. **b**, Gene expression programs induced in phagocytes by the apoptotic secretome. Display shows the differentially regulated genes (1,852 total, 886 upregulated, 966 downregulated), categorized per known or predicted function(s), literature and sequence similarity. Circle size is proportional to the number of differentially expressed genes ( $n = 4$ ) ( $P < 0.05$ ). OXPHOS, oxidative phosphorylation; UPR, unfolded protein response. **c**,

Differentially regulated genes in phagocytes in response to apoptotic cell supernatants with or without inhibition of the PANX1 channel (82 upregulated, 28 downregulated) ( $n = 4$ ). **d**, Validation of genes regulated by PANX1-dependent metabolites. LR73 cells were incubated with indicated supernatants for 4 h, and expression of *Areg* ( $n = 7$ ), *Nr4a1* ( $n = 7$ ), *Uap1* ( $n = 4$ ), and *Pbx1* ( $n = 5$ ) was determined in phagocytes by qPCR. AU, arbitrary units. \* $P = 0.014$ , \*\* $P = 0.009$ , \*\*\* $P = 0.0008$ , \*\*\*\* $P = 0.0001$ , one-way ANOVA with Turkey's multiple comparison test. Data are mean  $\pm$  s.e.m.

together with commonly used analysis software, revealed that the apoptotic secretome altered gene programs linked to cytoskeletal rearrangements, inflammation, wound healing or tissue repair, anti-apoptotic functions, metabolism and the regulation of cell size within the phagocyte (Fig. 3b), providing a molecular and metabolic basis for how apoptosis may influence essential tissue processes.

By comparing gene programs induced in live cells by supernatants from apoptotic cells versus conditions with genetic inhibition of PANX1, we identified 110 genes as differentially regulated on phagocytes by PANX1-dependent apoptotic metabolites (82 up and 28 down) (Fig. 3c); these include genes involved in anti-inflammatory processes, anti-apoptotic pathways, metabolism, and actin rearrangement (Fig. 3c). Secondary validation via quantitative PCR (qPCR) indicates that PANX1-dependent metabolites can alter genes linked to anti-inflammatory roles in phagocytes (*Nr4a1* and *Pbx1*)<sup>18,19</sup>, wound healing (*Areg* and *Ptgs2*)<sup>20,21</sup>, and metabolism (*Slc14a1*, *Sgk1* and *Uap1*)<sup>15,22</sup> (Fig. 3d, Extended Data Fig. 9b). Furthermore, filtration of supernatants through 3-kDa filters before the addition to phagocytes showed similar changes in gene transcription (Extended Data Fig. 9c), ruling out larger proteins or vesicles from dying cells. Thus, metabolites released from apoptotic cells, a subset of which is released in a PANX1-dependent manner, can alter selective gene programs in the surrounding cells that sense these metabolic signals.

To test whether apoptotic PANX1-dependent metabolites can induce gene expression changes in tissue phagocytes in vivo, we used *Panx1*<sup>fl/fl</sup>

*Cd4-cre* mice<sup>11</sup>, in which *Panx1* is targeted for deletion only within the thymocytes and not the thymic myeloid cells (Extended Data Fig. 10a, left). After confirming that *Panx1* was not deleted in the macrophages and dendritic cells (Extended Data Fig. 10a, right), and that comparable dexamethasone-induced thymocyte apoptosis occurs in control and *Panx1*<sup>fl/fl</sup>*Cd4-cre* mice (Extended Data Fig. 10b, c), we isolated CD11b<sup>+</sup> macrophages and CD11c<sup>+</sup> dendritic cells from the thymus and analysed changes in gene expression (Extended Data Fig. 10d, e). In wild-type mice, dexamethasone-induced apoptosis of thymocytes resulted in increased expression of *Uap1*, *Ugdh* and *Pbx1* in surrounding live myeloid cells (linked to anti-inflammatory macrophage skewing or glycosylation and transcription of *Il10*)<sup>19,23</sup> (Fig. 4a). This response was attenuated in mice lacking PANX1 channels in the dying thymocytes (Fig. 4a). Thus, apoptotic PANX1-dependent metabolites can induce gene expression changes in the surrounding tissue myeloid cells in vivo.

When tested individually, many of the metabolites did not strongly induce anti-inflammatory and tissue-repair genes from the RNA-seq (not shown). As these metabolites are concurrently released from apoptotic cells (Fig. 1), we then tested mixtures of six out of the eight PANX1-dependent metabolites (Fig. 2b) in two combinations: (i) spermidine, fructose-1,6-bisphosphate (FBP), dihydroxyacetone phosphate (DHAP), UDP-glucose, GMP and inosine-5'-monophosphate (IMP); and (ii) spermidine, GMP and IMP (Fig. 4b). All six have been previously administered in vivo in mice or rats without toxicity (Supplementary Table 4). We excluded AMP and glycerol-3-phosphate, as AMP can

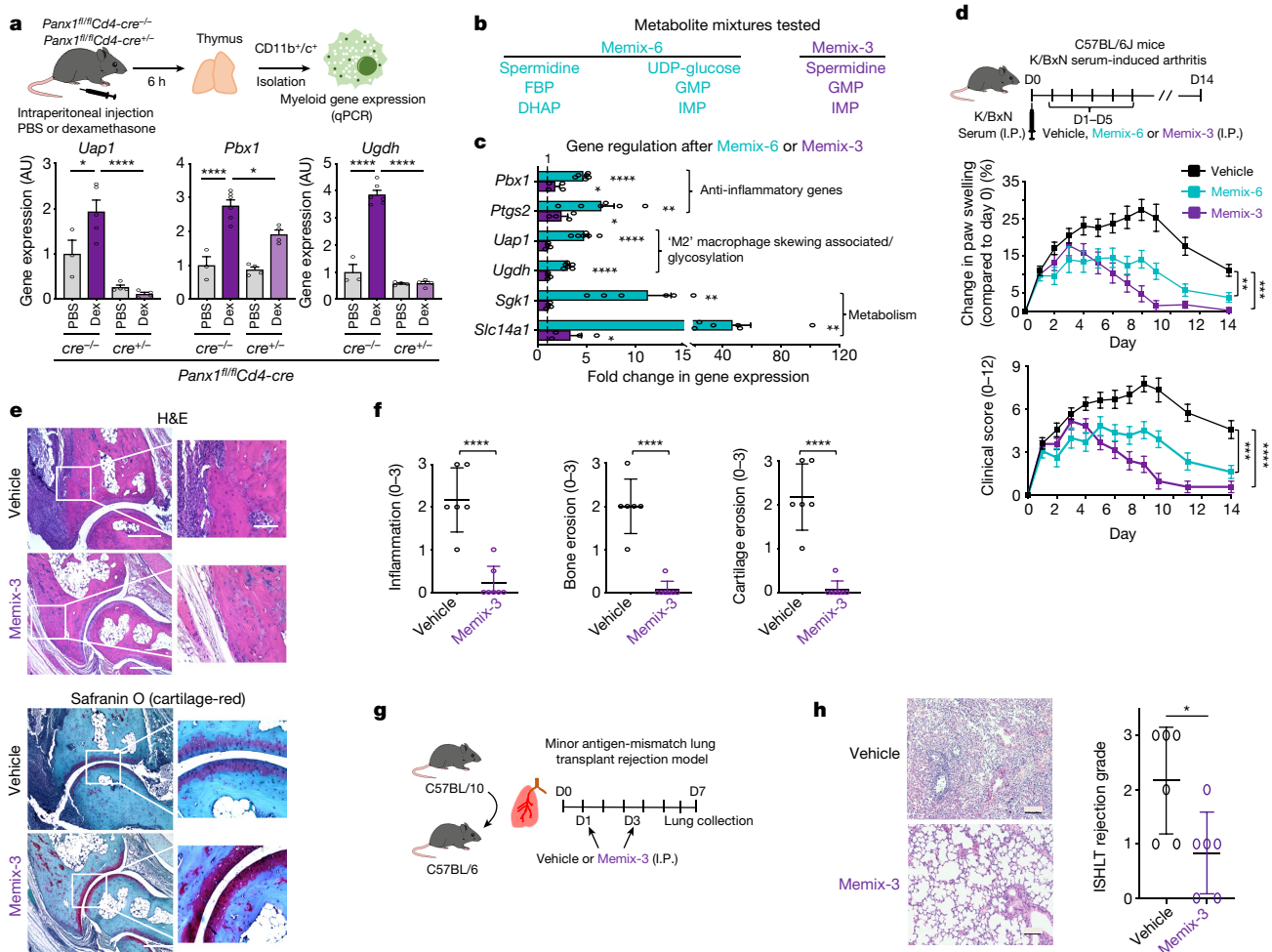


**Fig. 4 | PANX1-dependent metabolite release during apoptosis modulates phagocyte gene expression in vivo and can alleviate inflammation.** **a**, PANX1 expression in apoptotic thymocytes influences gene expression in myeloid cells in vivo. Control mice (*Panx1<sup>fl/fl</sup>Cd4-cre<sup>-/-</sup>*) or mice lacking PANX1 in thymocytes (*Panx1<sup>fl/fl</sup>Cd4-cre<sup>+/-</sup>*) were injected with dexamethasone (Dex) to induce apoptosis in thymocytes (*cre<sup>-/-</sup>* PBS  $n=3$ , *cre<sup>-/-</sup>* Dex  $n=6$ , *cre<sup>+/-</sup>* PBS, Dex  $n=4$ ). After 6 h, CD11b<sup>+</sup> CD11c<sup>+</sup> phagocytes were purified for qPCR analysis of *Uap1* ( $*P=0.032$ ,  $****P<0.0001$ ), *Pbx1* ( $****P=0.0001$ ,  $*P=0.0103$ ), and *Ugdh* ( $****P<0.0001$ ).  $P$  values were determined by one-way ANOVA with Turkey's multiple comparison test. **b**, PANX1-dependent release of metabolites from apoptotic cells was compared across cell types and apoptotic conditions to design different metabolite mixtures, Memix-6 (blue) and Memix-3 (purple). **c**, Memix-6 ( $n=6$ ) and Memix-3 ( $n=4$ ) solutions mimic gene expression changes in phagocytes induced by apoptotic supernatants.  $*P<0.05$ ,  $**P<0.01$ ,  $****P<0.0001$ , unpaired two-tailed Student's  $t$ -test. **d**, Top, schematic of arthritis induction and treatments (vehicle  $n=16$ , Memix-6  $n=11$ , Memix-3  $n=12$  mice). I.P., intraperitoneal. Middle, paw swelling was measured using a calliper and reported as the percentage change compared to day 0.

$**P=0.0028$ ,  $***P=0.0003$ . Bottom, scores were assessed on a scale of 1 to 4 per paw.  $**P=0.0004$ ,  $****P=0.0001$ .  $P$  values determined by two-way ANOVA. **e**, Ankle inflammation and bone erosion were scored via haematoxylin and eosin (H&E) staining (left) and safranin O staining (right), respectively, from arthritic mouse paws on day 8 ('peak' disease). Increased magnifications of affected areas are shown. Scale bars, 0.4 mm (main panel), 0.1 mm (magnification). **f**, Clinical analysis of inflammation (left), bone erosion (middle) and cartilage erosion (right) was scored by an investigator blinded to treatments (vehicle  $n=6$ , Memix-3  $n=7$ ).  $****P<0.0001$ , unpaired two-tailed Student's  $t$ -test. **g**, Memix-3 metabolite solution alleviates inflammation in a minor antigen-mismatch lung transplant model. Orthotopic left lung transplantation from C57BL/10 mice into C57BL/6 recipient mice, with Memix-3 administered on post-operation day 1 and 3. Lungs were obtained for histological scoring on day 7. **h**, H&E staining (left) and ISHLT rejection score<sup>28</sup> (right) in mice as in **g** (vehicle  $n=6$ , Memix-3  $n=6$ ).  $*P=0.024$ , unpaired two-tailed Student's  $t$ -test. Data are mean  $\pm$  s.e.m. (**a**, **c**, **d**) or mean  $\pm$  s.d. (**f**, **h**). Scale bars, 100  $\mu$ m.

be converted to adenosine, a known anti-inflammatory metabolite, and it was difficult to determine the optimal in vivo dose for glycerol-3-phosphate. The metabolite mixtures were quite potent in inducing gene expression in vitro, including genes linked to anti-inflammatory macrophage skewing or glycosylation (*Uap1* and *Ugdh*)<sup>23</sup>, transcription of *IL10* and inflammation resolution (*Pbx1*<sup>19</sup> and *Ptgs2*<sup>24</sup>), and metabolic processes (*Slc14a1* and *Sgk1*), some of which have also been shown to be involved in phagocytosis<sup>15</sup> (Fig. 4c). For simplicity, we have denoted the metabolite mixtures as 'Memix-6' and 'Memix-3' (Fig. 4b).

Given the anti-inflammatory gene signature induced by the metabolites, we next tested whether the Memix-6 and/or Memix-3 metabolites

attenuated inflammation in vivo in two contexts: a model of inflammatory arthritis and a model of lung-transplant rejection. In the arthritis model, a single injection of serum from arthritic transgenic K/BxN mice into C57BL/6J mice results in inflammation of the joints with progressive arthritic symptoms, followed by disease resolution<sup>25</sup>. Of relevance to our question, this arthritis model is dependent on myeloid cells<sup>25</sup>, with apoptosis known to occur during disease. We first asked whether the full apoptotic secretome could alleviate inflammation in this arthritis model, and found that this was the case (Extended Data Fig. 10f). Administration of Memix-6 or Memix-3 metabolites after the induction of arthritis when the disease symptoms are already noticeable

resulted in significant attenuation of paw swelling and other arthritic parameters, compared with treatment with vehicle controls (Fig. 4d). Because FBP alone can have ameliorative roles in arthritis<sup>26</sup>, we further tested Memix-3, which does not contain FBP. Memix-3 metabolites not only alleviated paw swelling and external clinical arthritis parameters, but also significantly protected the joints from inflammation, bone erosion and cartilage erosion (Fig. 4e, f).

We also tested Memix-3 in a model of lung-transplant rejection, in which local innate and adaptive immune responses orchestrated by graft-resident antigen-presenting myeloid cells dictate graft acceptance or rejection. We transplanted allografts from the left lung of C57BL/10 mice to a minor antigen-mismatched C57BL/6 recipient<sup>27</sup> (Fig. 4g), and treated the graft recipients with Memix-3 or saline vehicle control on post-operative days 1 and 3. On day 7 after engraftment, the control mice treated with saline showed severe acute rejection of allografts<sup>28</sup>. Notably, mice treated with Memix-3 had only minimal inflammation in the transplanted lungs (Fig. 4h), suggestive of amelioration of lung rejection. Complementary flow cytometric analysis of the lung showed reduced CD4 and CD8 cells in the transplanted lungs of mice treated with Memix-3 (data not shown). Thus, a subset of apoptotic metabolites can be harnessed for beneficial effects in two different inflammatory settings in vivo.

Collectively, the data presented here advance several concepts. First, we identify specific metabolites that are released from apoptotic cells (different cell types and modes of apoptosis induction); the specificity could arise from metabolic changes in the apoptotic cells (for example, sustained production of spermidine), and/or the opening of specific channels (such as PANX1). Second, apoptotic cells are not inert corpses awaiting removal; instead, via the release of metabolites as good-bye signals they actively modulate several gene programs in the neighbouring cells within a tissue. Third, the ability of a cocktail of apoptotic metabolites to attenuate arthritic symptoms and the rejection of lung transplantation provide a proof-of-concept that it is possible to harness the beneficial therapeutic properties of apoptosis in specific inflammatory conditions.

## Online content

Any methods, additional references, Nature Research reporting summaries, source data, extended data, supplementary information, acknowledgements, peer review information; details of author contributions and competing interests; and statements of data and code availability are available at <https://doi.org/10.1038/s41586-020-2121-3>.

1. Fuchs, Y. & Steller, H. Programmed cell death in animal development and disease. *Cell* **147**, 742–758 (2011).
2. Rothlin, C. V., Carrera-Silva, E. A., Bosurgi, L. & Ghosh, S. TAM receptor signaling in immune homeostasis. *Annu. Rev. Immunol.* **33**, 355–391 (2015).

3. Lindsten, T. et al. The combined functions of proapoptotic Bcl-2 family members bak and bax are essential for normal development of multiple tissues. *Mol. Cell* **6**, 1389–1399 (2000).
4. Gregory, C. D. & Pound, J. D. Cell death in the neighbourhood: direct microenvironmental effects of apoptosis in normal and neoplastic tissues. *J. Pathol.* **223**, 178–195 (2011).
5. Ryoo, H. D., Gorenc, T. & Steller, H. Apoptotic cells can induce compensatory cell proliferation through the JNK and the Wingless signaling pathways. *Dev. Cell* **7**, 491–501 (2004).
6. Ke, F. F. S. et al. Embryogenesis and adult life in the absence of intrinsic apoptosis effectors BAX, BAK, and BOK. *Cell* **173**, 1217–1230.e17 (2018).
7. Medina, C. B. & Ravichandran, K. S. Do not let death do us part: 'find-me' signals in communication between dying cells and the phagocytes. *Cell Death Differ.* **23**, 979–989 (2016).
8. Elliott, M. R. et al. Nucleotides released by apoptotic cells act as a find-me signal to promote phagocytic clearance. *Nature* **461**, 282–286 (2009).
9. Van Opendenbosch, N. et al. Caspase-1 engagement and TLR-induced c-FLIP expression suppress ASC/caspase-8-dependent apoptosis by inflammasome sensors NLRP1b and NLRC4. *Cell Rep.* **21**, 3427–3444 (2017).
10. Chekeni, F. B. et al. Pannexin 1 channels mediate 'find-me' signal release and membrane permeability during apoptosis. *Nature* **467**, 863–867 (2010).
11. Poon, I. K. H. et al. Unexpected link between an antibiotic, pannexin channels and apoptosis. *Nature* **507**, 329–334 (2014).
12. Good, M. E. et al. Pannexin 1 channels as an unexpected new target of the anti-hypertensive drug spironolactone. *Circ. Res.* **122**, 606–615 (2018).
13. Madeo, F., Eisenberg, T., Pietrocola, F. & Kroemer, G. Spermidine in health and disease. *Science* **359**, eaan2788 (2018).
14. Liu, X. et al. PNPT1 release from mitochondria during apoptosis triggers decay of poly(A) RNAs. *Cell* **174**, 187–201.e12 (2018).
15. Morioka, S. et al. Efferocytosis induces a novel SLC program to promote glucose uptake and lactate release. *Nature* **563**, 714–718 (2018).
16. Wang, Y. et al. Mitochondrial fission promotes the continued clearance of apoptotic cells by macrophages. *Cell* **171**, 331–345.e22 (2017).
17. Perry, J. S. A. et al. Interpreting an apoptotic corpse as anti-inflammatory involves a chloride sensing pathway. *Nat. Cell Biol.* **21**, 1532–1543 (2019).
18. Ipseiz, N. et al. The nuclear receptor Nr4a1 mediates anti-inflammatory effects of apoptotic cells. *J. Immunol.* **192**, 4852–4858 (2014).
19. Chung, E. Y. et al. Interleukin-10 expression in macrophages during phagocytosis of apoptotic cells is mediated by homeodomain proteins Pbx1 and Prep-1. *Immunity* **27**, 952–964 (2007).
20. Zaiss, D. M. W., Gause, W. C., Osborne, L. C. & Artis, D. Emerging functions of amphiregulin in orchestrating immunity, inflammation, and tissue repair. *Immunity* **42**, 216–226 (2015).
21. Goessling, W. et al. Genetic interaction of PGE2 and Wnt signaling regulates developmental specification of stem cells and regeneration. *Cell* **136**, 1136–1147 (2009).
22. Shayakul, C., Cléménçon, B. & Hediger, M. A. The urea transporter family (SLC14): physiological, pathological and structural aspects. *Mol. Aspects Med.* **34**, 313–322 (2013).
23. Jha, A. K. et al. Network integration of parallel metabolic and transcriptional data reveals metabolic modules that regulate macrophage polarization. *Immunity* **42**, 419–430 (2015).
24. Scher, J. U. & Pillinger, M. H. The anti-inflammatory effects of prostaglandins. *J. Invest. Med.* **57**, 703–708 (2009).
25. Korganow, A. S. et al. From systemic T cell self-reactivity to organ-specific autoimmune disease via immunoglobulins. *Immunity* **10**, 451–461 (1999).
26. Veras, F. P. et al. Fructose 1,6-bisphosphate, a high-energy intermediate of glycolysis, attenuates experimental arthritis by activating anti-inflammatory adenosinergic pathway. *Sci. Rep.* **5**, 15171 (2015).
27. Krupnick, A. S. et al. Orthotopic mouse lung transplantation as experimental methodology to study transplant and tumor biology. *Nat. Protocols* **4**, 86–93 (2009).
28. Stewart, S. et al. Revision of the 1996 working formulation for the standardization of nomenclature in the diagnosis of lung rejection. *J. Heart Lung Transplant* **26**, 1229–1242 (2007).

**Publisher's note** Springer Nature remains neutral with regard to jurisdictional claims in published maps and institutional affiliations.

© The Author(s), under exclusive licence to Springer Nature Limited 2020

## Methods

### Reagents

Trovafoxacin, spironolactone, dexamethasone, spermidine, FBP, DHAP, IMP and GMP were obtained from Sigma. UDP-glucose was obtained from Abcam, and annexin V-Pacific Blue was from BioLegend. 7AAD, TO-PRO-3 anti-CD11b-PE (clone M1/70), anti-CD11c-PE (clone N418), and anti-CD16/CD32 (clone 93) were obtained from Invitrogen. Antibodies specific for mouse CD95 were obtained from BD. Human anti-Fas (clone CH11) was obtained from Millipore. Other reagents were obtained as follows: ABT-737 (abcam), TRAIL (Sigma) and zVAD-FMK (Enzo).

### Mice

C57BL/10 and C57BL/6J wild-type mice were acquired from Jackson Laboratories. *Panx1<sup>fl/fl</sup>* and *Panx1<sup>-/-</sup>* mice have previously been described<sup>11</sup>. To generate mice with deletion of *Panx1* in thymocytes, *Panx1<sup>fl/fl</sup>* mice were crossed to *Cd4-cre* mice (Taconic). KRN T cell receptor (TCR) transgenic mice were a gift from D. Mathis and were bred to non-obese diabetic (NOD) mice (Jackson Laboratories) to obtain the K/BxN mice, which develop progressive spontaneous arthritis<sup>29</sup>. Serum was collected from 9-week-old K/BxN mice by cardiac puncture. Animal procedures were approved and performed according to the Institutional Animal Care and Use Committee (IACUC) at the University of Virginia.

### Apoptosis induction

Wild-type Jurkat E6.1 (ATCC) or dominant-negative PANX1-expressing (PANX1-DN)<sup>10</sup> cells were resuspended in RPMI-1640 containing 1% BSA, 1% penicillin-streptomycin-glutamine (PSQ), and 10 mM HEPES and treated with 250 ng ml<sup>-1</sup> anti-Fas (clone CH11), 10 μM ABT-737, or exposed to 150 mJ cm<sup>-2</sup> UV-C irradiation for 1–2 min (Stratalinker). Jurkat cells were incubated for 4 h after apoptosis induction. For apoptosis induction in the presence of PANX1 inhibitors, Jurkat cells were treated with spironolactone (50 μM) or trovafoxacin (25 μM) in RPMI containing 1% BSA and 1% PSQ.

Primary thymocytes isolated from 4–6-week-old wild-type or *Panx1<sup>-/-</sup>* mice were treated with 5 μg ml<sup>-1</sup> anti-Fas (clone Jo2), that was subsequently crosslinked with 2 μg ml<sup>-1</sup> protein G. Primary thymocytes were incubated for 1.5 h after apoptosis induction.

BMDMs from *B6<sup>Nlrp1b<sup>+</sup></sup> CI<sup>-/-</sup> CII<sup>-/-</sup>* mice (C57BL/6J mice that express a functional *Nlrp1b* transgene (*B6<sup>Nlrp1b<sup>+</sup></sup>*)) crossed with mice lacking caspase-1 (*CI*, also known as *Casp1*) and caspase-11 (*CII*, also known as *Casp4*) were a gift from M. Lamkanfi's laboratory. BMDMs were generated by culturing mouse bone marrow cells in RPMI medium conditioned with 10% dialysed serum and 1% penicillin-streptomycin. The medium was supplemented with 20 ng ml<sup>-1</sup> of purified mouse M-CSF. Cells were incubated in a humidified atmosphere containing 5% CO<sub>2</sub> for 6 days. BMDMs from wild-type B6 or *B6<sup>Nlrp1b<sup>+</sup></sup> CI<sup>-/-</sup> CII<sup>-/-</sup>* mice were seeded in 6-well plates and, the next day, either left untreated or stimulated with 500 ng ml<sup>-1</sup> anthrax protective antigen (500 ng ml<sup>-1</sup>, Quadrtech) and anthrax lethal factor (250 ng ml<sup>-1</sup>, Quadrtech). Supernatants from either untreated or treated BMDMs were collected. Cellular debris was removed via centrifugation, and the clarified supernatant was used for metabolic profiling.

A549 cells were treated with 10 μM ABT-737 or exposed to 600 mJ cm<sup>-2</sup> UV irradiation, and incubated for 24 h. HCT-116 cells were treated with 10 μM ABT-737 or 100 ng ml<sup>-1</sup> TRAIL and incubated for 24 h. All cells were pre-treated for 10 min with 50 μM zVAD before apoptosis induction in indicated experiments. All cells were incubated at 37 °C with 5% CO<sub>2</sub> for indicated times.

### Metabolite detection

Spermidine detection was measured using a colorimetric kit (Cloud-Clone) via manufacturer's protocol. In brief, supernatants taken from cells under specified conditions were centrifuged at 1,000g for 20 min.

All reagents were brought to room temperature before use. Then, 50 μl of sample was added to each well followed by equal volume of detection reagent A and the plate was mixed. Samples were incubated covered for 1 h at 37 °C. Wells were washed with wash solution three times before the addition of detection reagent B, after which samples were incubated for another 30 min at 37 °C. Samples were washed five more times. Substrate solution (90 μl) was then added to each well and incubated for 10 min at 37 °C, after which stop solution (50 μl) was added, and the plate was mixed and immediately measured at 450 nm on a plate reader (Flex Station 3). Analysis was performed by back calculation to the standard curve, background subtraction and normalization to live cell controls.

ATP was measured using a luciferase-based kit (Promega) via the manufacturer's protocol. All reagents were equilibrated to room temperature before use. In brief, supernatants taken from cells under specified conditions were immediately moved to ice, and centrifuged at 500g for 5 min. Samples were placed back on ice and 50 μl of samples and 50 μl of luciferase reagent were mixed in a 96-well opaque plate. Luminescence was immediately measured on the Flex Station 3. Analysis was performed by back calculation to the standard curve, background subtraction and normalization to live cell controls.

Glycerol-3-phosphate and creatine were measured on the basis of manufacturers' protocols (Abcam). In brief, supernatants were taken from specified culture conditions and spun at 500g. Then, 50 μl of supernatant was added to a 96-well plate. Detection reagents were prepared as indicated in the protocol and added to respective wells. Samples were incubated for 40 min or 1 h for glycerol-3-phosphate or creatine, respectively. Absorbance at 450 nm or fluorescence at excitation/emission 535/587 nm was measured for glycerol-3-phosphate or creatine, respectively.

### Flow cytometry of apoptosis and PANX1 activation

Apoptotic cells were stained with annexin V-Pacific Blue, 7AAD and TO-PRO-3 for 15 min at room temperature in annexin V binding buffer (140 mM NaCl, 2.5 μM CaCl, 10 mM HEPES) and subjected to flow cytometry on Attune NxT (Invitrogen). Data were analysed using FlowJo v.10 software.

### Metabolomics analysis of apoptotic supernatant and cell pellet

Sample extraction, processing, compound identification, curation and metabolomic analyses were carried out at Metabolon and Human Metabolome Technologies (HMT)<sup>30</sup>. In brief, supernatants were separated from cell pellets via sequential centrifugation and frozen before shipment for metabolomic analysis. For HMT, supernatant samples were spiked with 10 μl of water with internal standards, then filtered through a 5-kDa cut-off filter to remove macromolecules and small vesicles. Cationic compounds were diluted and measured using positive ion mode electrospray ionization (ESI) via capillary electrophoresis–time-of-flight mass spectrometry (CE–TOF/MS). Anionic compounds were measured in the positive or negative ion mode ESI using capillary electrophoresis–tandem mass spectrometry (CE–MS/MS). Samples were diluted to improve the capillary electrophoresis–triple quadrupole mass spectrometry (CE–QqQMS) analysis. Peak identification and metabolite quantification were determined using migration time, mass-to-charge ratio, and the peak area normalized to the internal standard and standard curves. Concentrations reported are on a per million cell basis, which was derived by back calculations on the cell number that was used in the experimental set-up.

For untargeted metabolomics analysis by Metabolon, recovery standards were added to samples to monitor quality control of the analysis. Samples were precipitated in methanol with shaking for 2 min. Samples were then placed on the TurboVap to remove organic solvent and the samples were stored overnight under nitrogen gas. Samples were analysed under four different conditions; two for analysis by two separate reverse phase (RP)/ultra-performance liquid chromatography

# Article

(UPLC)–MS/MS methods with positive ion mode ESI, one for analysis by RP/UPLC–MS/MS with negative ion mode ESI, and one for analysis by HILIC/UPLC–MS/MS with negative ion mode ESI. Using a library based on authenticated standards that contains the retention time/index, mass-to-charge ratio ( $m/z$ ), and chromatographic data (including MS/MS spectral data) on all molecules in the library (Metabolon), the metabolite identification could be performed with reverse scores between the experimental data and authenticated standards. Although there may be similarities based on one of these factors, the use of all three data points can be used to identify biochemicals.

## Metabolite flux experiments with [ $^{13}\text{C}$ ]arginine labelling

Cells were re-suspended in arginine-free RPMI medium containing 10% dialysed serum, supplemented with 1 mM  $^{13}\text{C}_6$ -labelled L-arginine HCl (Thermo Fischer Scientific). Cells were either exposed to UV or left untreated. This step was performed within 1 min of the addition of medium containing [ $^{13}\text{C}$ ]arginine to cells. Cells were then incubated at 37 °C. Samples were collected every hour to trace the incorporation of the label from arginine into the polyamine pathway for both UV-exposed and live cells. Where indicated, cells were pre-treated with zVAD-FMK to inhibit caspases.

Metabolite extraction from the pellet or supernatant was performed by adding 300  $\mu\text{l}$  of 6% trichloroacetic acid (TCA) to a pellet of 4 million cells on ice. The samples were then vortexed thoroughly at 4 °C, followed by centrifugation to remove cell debris. Supernatant (100  $\mu\text{l}$ ) was mixed with  $\text{Na}_2\text{CO}_3$  (900  $\mu\text{l}$  of 0.1 M, pH 9.3), followed by isobutyl chloroformate addition (25  $\mu\text{l}$ ). The mixture was incubated at 37 °C for 30 min and then centrifuged for 10 min at 20,000g. Supernatant (800  $\mu\text{l}$ ) was transferred to a fresh tube, followed by the addition of 1,000  $\mu\text{l}$  diethyl ether and vortexing. The mixture was allowed to sit at room temperature for 10 min for phase separation after which, 900  $\mu\text{l}$  of sample was collected in a fresh Eppendorf tube. The samples were dried via Speedvac. For liquid chromatography–mass spectrometry (LC–MS) analysis, 150  $\mu\text{l}$  of 1:1 mixture of 0.2% acetic acid in water and 0.2% of acetic acid in acetonitrile was added to the dried sample.

## RNA-seq analysis

LR73 cells (ATCC) were plated at  $10^5$  per well in 24-well tissue culture plates and cultured for 16 h at 37 °C with 5%  $\text{CO}_2$ . The cells were then rinsed with PBS, and fresh supernatants taken from live Jurkat, apoptotic Jurkat (UV), or PANX1-DN apoptotic Jurkat (UV) cells were added for 4 h (as described in ‘Apoptosis induction’). Total RNA was collected using the Nucleospin RNA kit (Macherey-Nagel) and an mRNA library was constructed with Illumina TruSeq platform. Transcriptome sequencing using an Illumina NextSeq 500 cartridge was then performed on samples from four independent experiments. RNA-seq data were analysed using Rv1.0.136 and the R package DeSeq2 for differential gene expression, graphical representation, and statistical analysis.

## Quantitative reverse transcription PCR analysis

RNA was extracted from cells treated with different live or apoptotic supernatants. Where indicated, supernatants were filtered through a 3-kDa filter as suggested by manufacturer’s protocol. In brief, supernatants were separated from cells and large vesicles via sequential centrifugations. Supernatants were then added to 3-kDa filters (Millipore) and centrifuged for 1 h at 3,000g before the addition of supernatant to live LR73 cells. Nucleospin RNA kit (Macherey-Nagel) was used for RNA extraction and cDNA was synthesized using QuantiTect Reverse Transcription Kit (Qiagen). Gene expression of indicated genes was performed using Taqman probes (Applied Biosystems) and the StepOnePlus Real Time PCR System (Applied Biosystems).

## Thymocyte death induction in vivo

Six- to eight-week-old *Panx1<sup>fl/fl</sup>* or *Panx1<sup>fl/fl</sup> Cd4-cre* mice were injected intraperitoneally with dexamethasone (250  $\mu\text{g}$ ). Thymus was obtained

6 h after injection and single cell suspensions were prepared using 70- $\mu\text{m}$  strainers (Fisher). An aliquot of digested tissue was taken to measure the extent of thymocyte cell death and PANX1 activation using annexin V-Pacific Blue, 7AAD, and TO-PRO-3, as described in ‘Flow cytometry of apoptosis and PANX1 activation’. Samples were acquired on Attune NxT (Invitrogen) and analysed using FlowJo v.10 Software.

## Thymic myeloid cell isolation and gene expression

Six- to eight-week old *Panx1<sup>fl/fl</sup>* or *Panx1<sup>fl/fl</sup> Cd4-cre* mice were injected with dexamethasone and single cell suspensions of thymus were prepared as described above. After isolation, cells were incubated with anti-CD16/CD32 (Fc-Block, Invitrogen) for 20 min at 4 °C. Cells were then stained with anti-CD3-PE and run through a MACS kit using anti-PE microbeads to ‘de-bulk’ the cell suspension and remove most thymocytes. Cell flow-through (CD3-negative population) was collected and stained with anti-CD11b-PE and anti-CD11c-PE antibodies for 30 min at 4 °C. Stained cells were purified using the anti-PE MicroBeads MACS kit (Miltenyi Biotec), following the manufacturer’s protocol. Sample aliquots were run on the Attune NxT (Invitrogen) and analysed using FlowJo v.10 Software. Total RNA from purified cells was isolated Nucleospin RNA kit (Macherey-Nagel) for cDNA synthesis and quantitative reverse transcription PCR (qRT–PCR), as described in ‘Quantitative reverse transcription PCR analysis’.

## Memix preparation and in vivo treatment

The metabolite mixture Memix-6 was composed of the six metabolites: spermidine, FBP, DHAP, GMP, IMP and UDP-glucose. Memix-3 was composed of spermidine, GMP and IMP. Concentrations of metabolites used for in vitro LR73 phagocyte treatment were as follows (based on targeted metabolomics): IMP (3.3  $\mu\text{M}$ ), DHAP (36  $\mu\text{M}$ ), FBP (0.5  $\mu\text{M}$ ), GMP (2.1  $\mu\text{M}$ ), UDP-glucose (2  $\mu\text{M}$ ) and spermidine (0.3  $\mu\text{M}$ ). Concentrations of metabolites used for in vivo mice treatment were as follows: IMP (100  $\text{mg kg}^{-1}$ ), DHAP (50  $\text{mg kg}^{-1}$ ), FBP (500  $\text{mg kg}^{-1}$ ), GMP (100  $\text{mg kg}^{-1}$ ), UDP-glucose (100  $\text{mg kg}^{-1}$ ) and spermidine (100  $\text{mg kg}^{-1}$ ).

## K/BxN induced arthritis

C57BL/6J mice were given intraperitoneal injections of 150  $\mu\text{l}$  of serum from K/BxN mice on day 0 and paw swelling was measured at indicated time points using a calliper (Fisher). Measurements are presented as the percentage change from day 0. On day 1, mice were randomly assigned into three groups and given daily intraperitoneal injections of Memix-3, Memix-6 or vehicle up to day 5. In separate experiments, mice on day 1 were randomly assigned and given daily injections of either live or apoptotic supernatants up to day 5. Clinical scores were assigned for each paw as follows: 0, no paw swelling or redness observed; 1, redness of the paw or a single digit swollen, normal V shape of the hind foot (the foot at the base of the toes is wider than the heel and ankle); 2, two or more digits swollen or visible swelling of the paw, U shape of the hind foot (the ankle and the midfoot are equal in thickness); and 3, reversal of the V shape of the hind foot into an hourglass shape (the foot is wider at the heel than at the base of the toes). A combined clinical score of all paws is presented. Paw measurements and clinical score assignments were performed by an investigator blinded to the treatment groups.

## Lung transplant rejection model

Orthotopic left lung transplantation was carried out according to previous reports<sup>27</sup>. To study the alteration of allo-immune response by a minor antigen-mismatched combination, C57BL/10 donor and C57BL/6 recipient mice were used. The recipient mice were administered with Memix-3 or vehicle intraperitoneally on post-operative days 1 and 3. On day 7, the recipient mice were euthanized and left lung allografts were obtained and processed for histology.

## Histology

Lungs were fixed in formalin, sectioned and stained with H&E. The acute rejections were graded according to the International Society

for Heart and Lung Transplantation (ISHLT) A grade criteria by a lung pathologist who was blinded to the experimental settings<sup>28</sup>. For the model of arthritis, mice were euthanized at day 8 of K/BxN-serum-induced arthritis and the hind paws were fixed in 10% formalin (Fisher). Decalcification, sectioning, paraffin embedding, H&E staining and safranin O staining was performed by HistoTox Labs. Images of ankle sections were taken on an EVOS FL Auto (Fisher) and analysed using the accompanying software. Histology scoring was performed by an investigator blinded to the mouse treatment. For inflammation and cartilage erosion scoring, the following criteria were used: 0, none; 1, mild; 2, moderate; and 3, severe. For bone erosion scoring, the following criteria were used: 0, no bone erosions observed; 1, mild cortical bone erosion; 2, severe cortical bone erosion without the loss of bone integrity; and 3, severe cortical bone erosion with the loss of cortical bone integrity and trabecular bone erosion.

### Statistical analysis

Statistical significance was determined using GraphPad Prism 7, using unpaired Student's two-tailed *t*-test (paired and unpaired), one-way ANOVA, or two-way ANOVA according to test requirements. Grubbs' outlier test was used to determine outliers, which were excluded from final analysis. \**P* < 0.05, \*\**P* < 0.01, \*\*\**P* < 0.001. No statistical methods were used to predetermine sample size. Unless otherwise stated, experiments were not randomized and investigators were not blinded to allocation during experiments and outcome assessment.

### Reporting summary

Further information on research design is available in the Nature Research Reporting Summary linked to this paper.

### Data availability

RNA-seq data have been submitted to the Gene Expression Omnibus (GEO) under accession number GSE131906. Source Data for Figs. 1–4 and Extended Data Figs. 1–10 are provided with the paper. Other data

that support the findings of this study are available from the corresponding author upon request.

### Code availability

R code used for heat map generation, volcano plots and bioinformatic analysis is available from the corresponding author upon request.

29. Kouskoff, V. et al. Organ-specific disease provoked by systemic autoimmunity. *Cell* **87**, 811–822 (1996).
30. Evans, A. M., DeHaven, C. D., Barrett, T., Mitchell, M. & Milgram, E. Integrated, nontargeted ultrahigh performance liquid chromatography/electrospray ionization tandem mass spectrometry platform for the identification and relative quantification of the small-molecule complement of biological systems. *Anal. Chem.* **81**, 6656–6667 (2009).

**Acknowledgements** The authors thank members of the Ravichandran laboratory, and members of the Pannexin Interest Group at UVA for numerous discussions, and critical reading of the manuscript, and M. Lamkanfi for the *Nlrp1b* transgenic mice. This work is supported by grants to K.S.R. from NHLBI (P01HL120840), NIGMS R35GM122542, and the Center for Cell Clearance/University of Virginia School of Medicine, and the Odysseus Award from the FWO, Belgium, EOS Grant from the FWO (3083753-DECODE), and the NHLBI (P01HL120840) and NIAID (R21 AI139967 and R21 AI135455) to U.L. Additional support was received through the NIH T32 Pharmacology Training Grant (T32GM007055) (C.B.M. and B.B.), Mark Foundation Fellowship from the Cancer Research Institute and a K99 from the NCI (to J.S.A.P.), and the Kanye Foundation of Japan (to S.M.). Current address for Justin Perry: Immunology Program, Memorial Sloan-Kettering Cancer Center, New York, NY. P.M. is supported by a FWO-Senior postdoctoral fellowship.

**Author contributions** C.B.M. and K.S.R. designed the experiments. C.B.M. performed most experiments. P.M.M. performed the macrophage apoptosis and polyamine tracing experiments. S.A. and C.B.M. performed the arthritis experiments. J.S.A.P. assisted with the bioinformatic analyses. Y.G. and A.S.K. assisted with the lung transplant experiments. S.M., B.B. and S.W. provided experimental expertise on a few specific experiments. B.G. assisted with the polyamine mass spectrometry and U.L. provided mice and conceptual advice. C.B.M. and K.S.R. wrote the manuscript with input from co-authors.

**Competing interests** The authors declare no competing interests.

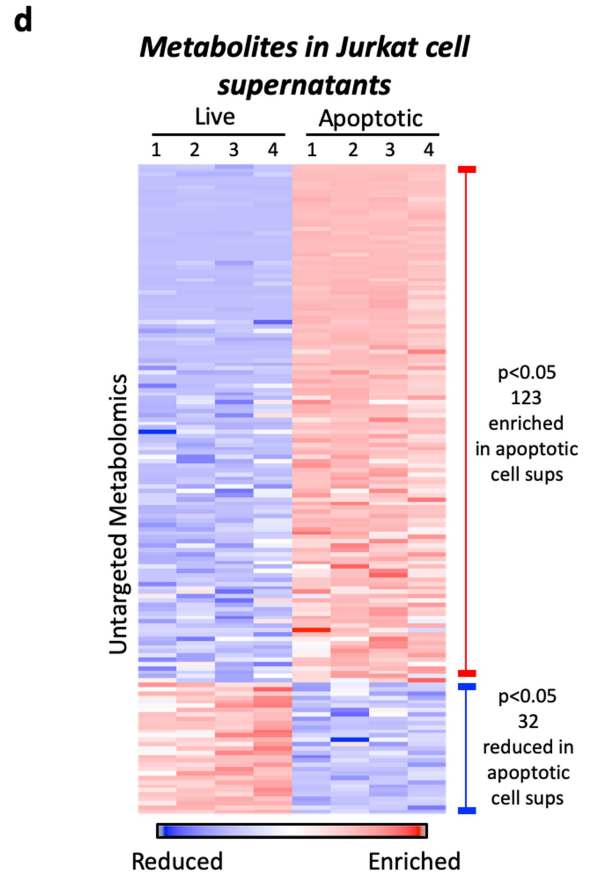
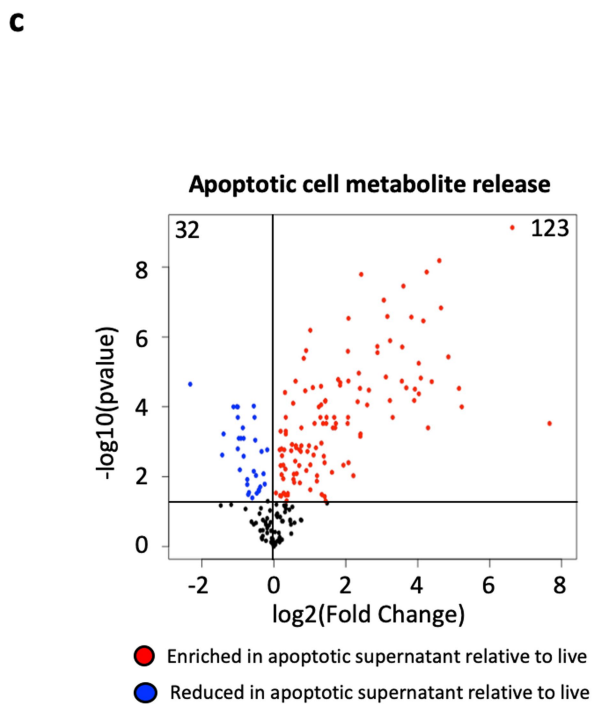
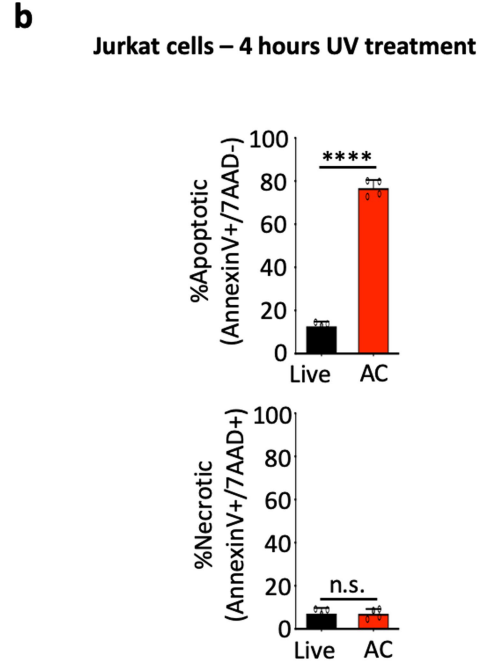
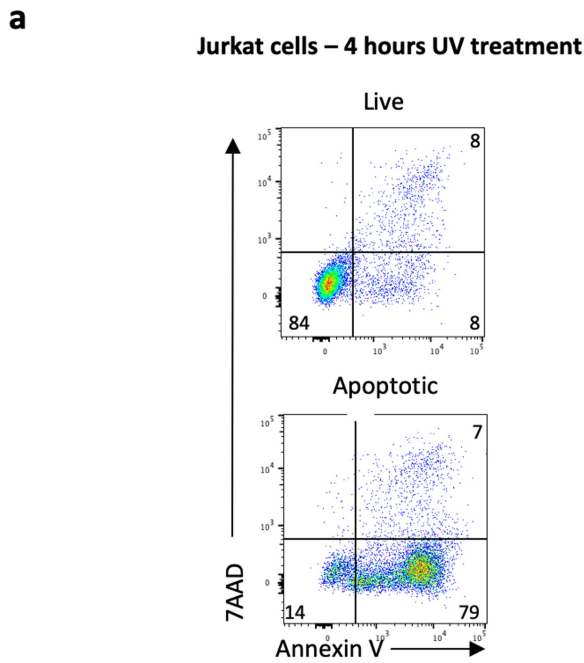
### Additional information

**Supplementary information** is available for this paper at <https://doi.org/10.1038/s41586-020-2121-3>.

**Correspondence and requests for materials** should be addressed to K.S.R.

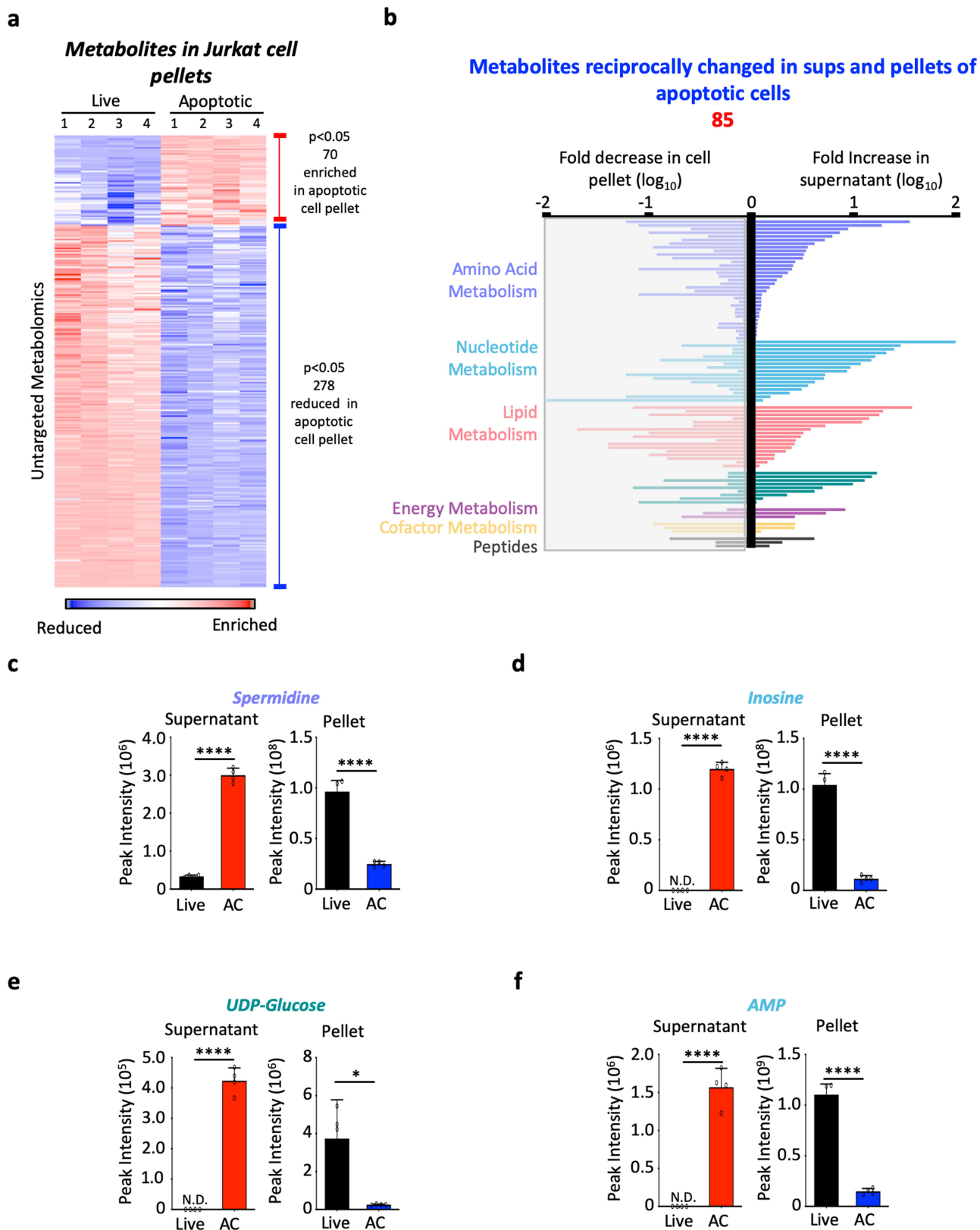
**Peer review information** Nature thanks Seamus Martin, Gary Siuzdak and the other, anonymous, reviewer(s) for their contribution to the peer review of this work.

**Reprints and permissions information** is available at <http://www.nature.com/reprints>.



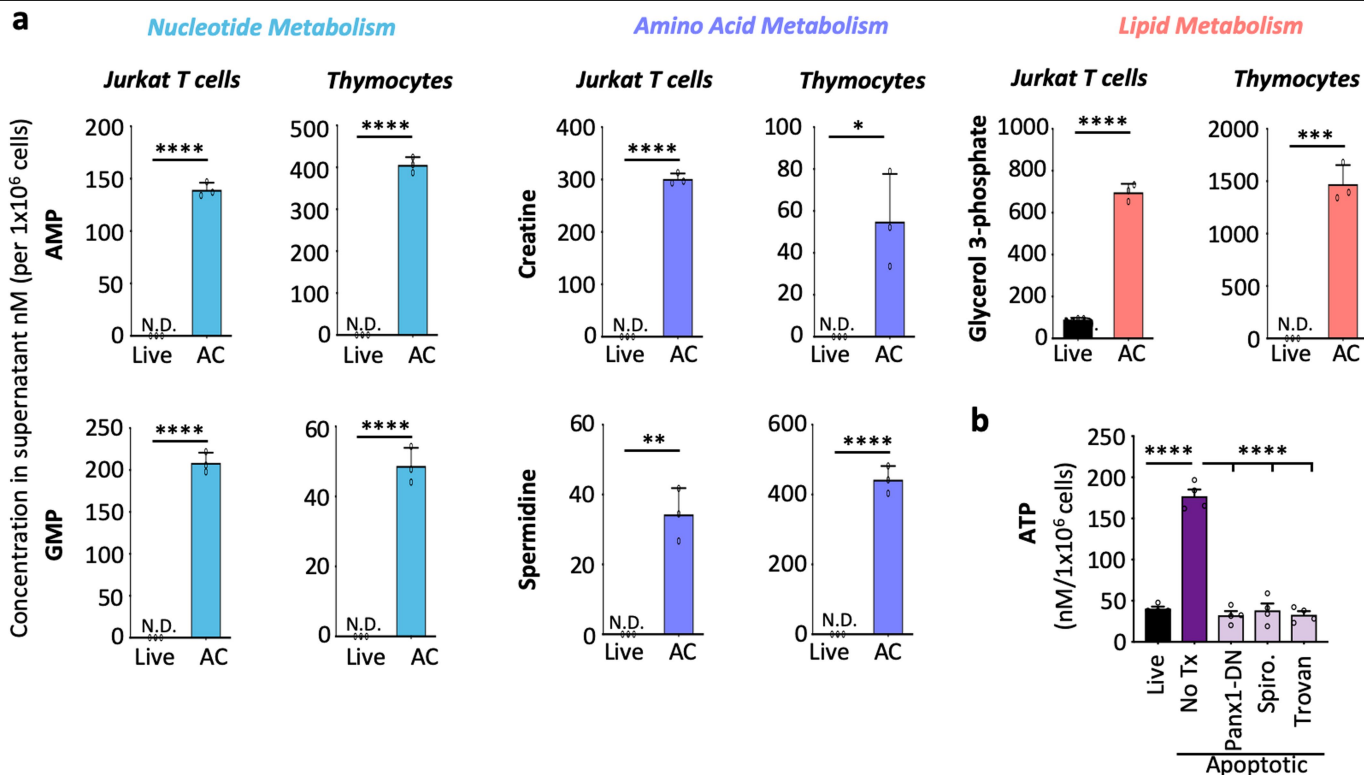
**Extended Data Fig. 1 | Metabolite release from apoptotic Jurkat cells.** **a**, Jurkat cells were induced to undergo apoptosis by UV irradiation. Staining with 7AAD and annexin V (AV) was used to determine the percentage of live (AV<sup>-</sup>7AAD<sup>-</sup>), apoptotic (AV<sup>+</sup>7AAD<sup>-</sup>) or necrotic (AV<sup>+</sup>7AAD<sup>+</sup>) cells after 4 h. **b**, Quantitative analysis of apoptosis (top) and secondary necrosis (bottom) ( $n=4$ ). Data are mean  $\pm$  s.d. \*\*\*\* $P < 0.0001$ , unpaired two-tailed Student's  $t$ -test.

**c, d**, Volcano plot (**c**) and heat map (**d**) from untargeted metabolomics of supernatants from Jurkat T cells, representing statistically enriched or reduced ( $P < 0.05$ , two-sided Welch's two-sample  $t$ -test) metabolites in the apoptotic supernatants relative to live supernatants. Data are representative of four biological replicates.



**Extended Data Fig. 2 | Reciprocal metabolite changes between apoptotic supernatant and pellet.** **a**, Heat map produced from untargeted metabolomics of Jurkat T cell pellets, representing statistically enriched or reduced ( $P < 0.05$ , two-sided Welch's two-sample  $t$ -test) metabolites in the apoptotic pellet relative to the live cell pellet ( $n = 4$  biologically independent samples). **b**, Bi-directional plot representing the 85 metabolites that were statistically enriched in the apoptotic supernatant and simultaneously

reduced in the apoptotic cell pellet relative to live cell conditions ( $P < 0.05$ , two-sided Welch's two-sample  $t$ -test). Metabolites were grouped by metabolic pathways ( $n = 4$  biologically independent samples). **c-f**, Mass spectrometry was used to determine the relative amount of spermidine (**c**), inosine (**d**), UDP-glucose (**e**) and AMP (**f**) in supernatants and cell pellets from Jurkat T cells in live and apoptotic conditions ( $n = 4$  biologically independent samples). \* $P = 0.014$ , \*\*\*\* $P < 0.0001$ , unpaired two-tailed Student's  $t$ -test. Data are mean  $\pm$  s.d.

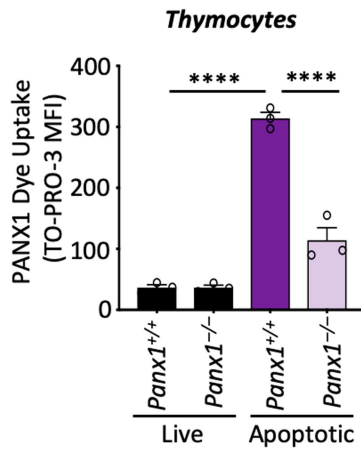
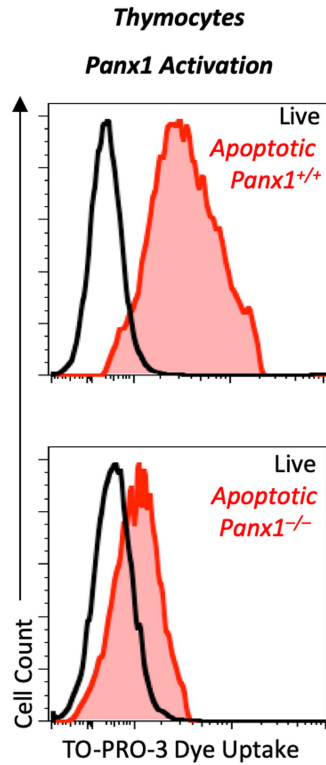
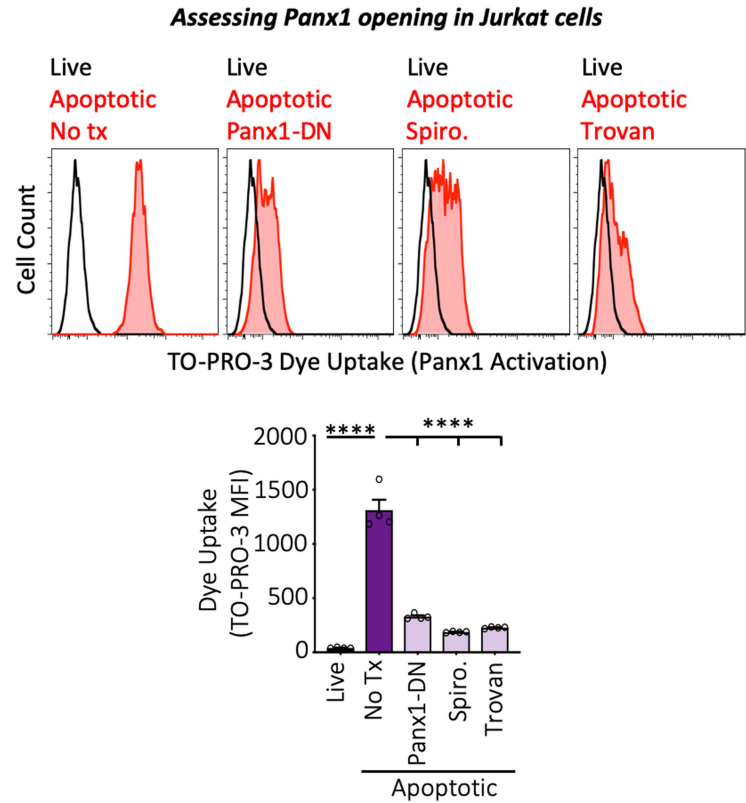


**c**

Cell Type	Apoptotic Stimulus	Approach	Metabolites Screened
1. Jurkat E6.1 (T cell)	UV	Untargeted Metabolomics	>3000
	Fas	Targeted Metabolomics	116
	ABT-737 (BH3 mimetic)	Colorimetric/Fluorometric Kit	ATP, Spermidine
2. Primary Thymocyte	Fas	Targeted Metabolomics	116
3. Primary BMDM	Anthrax Lethal Toxin	Untargeted Metabolomics	>3000
4. A549 (Lung epithelial cell)	UV	Colorimetric/Fluorometric Kit	ATP, Spermidine, G-3-P, Creatine
	ABT-737 (BH3 mimetic)	Colorimetric/Fluorometric Kit	ATP, Spermidine, G-3-P, Creatine
5. HCT116 (colonic epithelial cell)	ABT-737 (BH3 mimetic)	Colorimetric/Fluorometric Kit	ATP, Spermidine, G-3-P, Creatine
	TRAIL	Colorimetric/Fluorometric Kit	ATP, Spermidine, G-3-P, Creatine

**Extended Data Fig. 3 | Conserved metabolite release during apoptosis. a,** Mass spectrometry was used to measure the concentration of the five metabolites that were released across all conditions and platforms tested, in live or apoptotic supernatants per million Jurkat T cells or isolated primary thymocytes (back-calculated from total cells used in experimental set-up) ( $n=3$ ). Metabolites are grouped by metabolic pathways. Data are mean  $\pm$  s.d.  $^*P=0.014$ ,  $^{**}P=0.0014$ ,  $^{***}P=0.0002$ ,  $^{****}P<0.0001$ , unpaired two-tailed

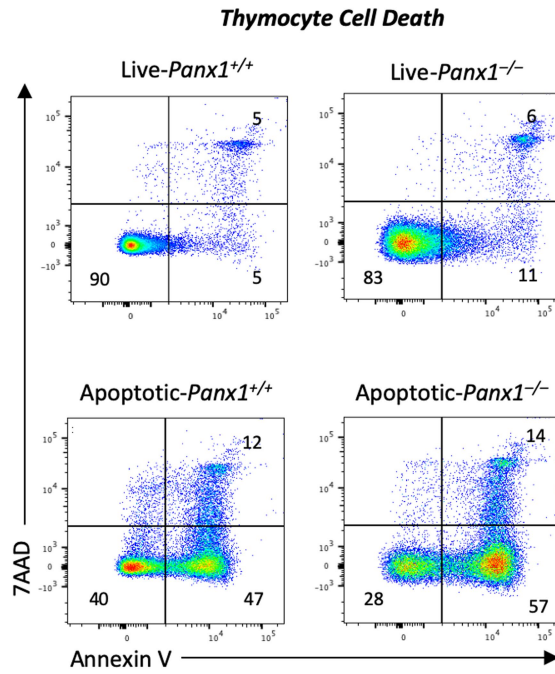
Student's  $t$ -test. **b,** The concentration of ATP released in the supernatant across the different apoptotic Jurkat cells was determined by luciferase assay ( $n=4$ ). Data are mean  $\pm$  s.e.m.  $^{****}P<0.0001$ , ordinary one-way ANOVA with Turkey's multiple comparison test. **c,** Table outlining the different cell types, apoptotic stimuli, techniques and metabolites screened for untargeted (more than 3,000 features or compounds) and targeted (116 metabolites) metabolomics, including ATP, spermidine, glycerol-3-phosphate and creatine.

**a****b**

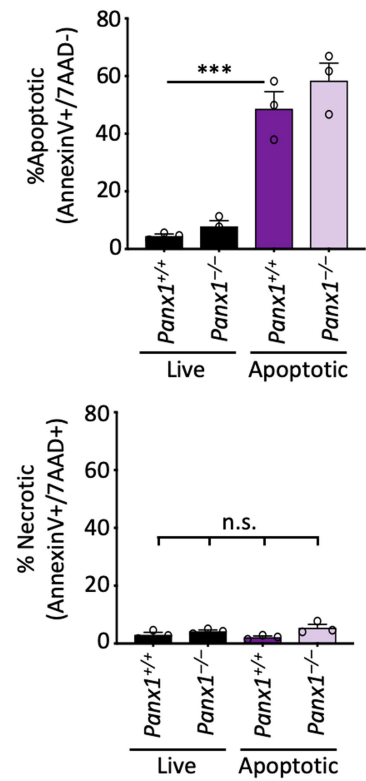
**Extended Data Fig. 4 | PANX1 activation and inhibition during cell death. a.** Top, representative histograms of TO-PRO-3 dye uptake in thymocytes across the different conditions. Bottom, PANX1 activation in live and apoptotic thymocytes from wild-type (*Panx1*<sup>+/+</sup>) and PANX1-knockout (*Panx1*<sup>-/-</sup>) mice as assessed via flow cytometry by measuring the mean fluorescent intensity of TO-PRO-3 dye uptake ( $n = 3$  biological replicates). Data are mean  $\pm$  s.e.m. \*\*\*\* $P < 0.0001$ , ordinary one-way ANOVA with Turkey's multiple comparison

test. **b.** Top, representative histograms of TO-PRO-3 dye uptake in Jurkat cells, across the different conditions described. Bottom, PANX1 activation as assessed by flow cytometry of the uptake of TO-PRO-3 dye in apoptotic wild-type Jurkat cells, Jurkat cells expressing mutant PANX1-DN, and Jurkat cells treated with PANX1 inhibitor spironolactone (50  $\mu$ M) or trovafloxacin (25  $\mu$ M) ( $n = 4$  biological replicates). Data are mean  $\pm$  s.e.m. \*\*\*\* $P < 0.0001$ , ordinary one-way ANOVA with Turkey's multiple comparison test.

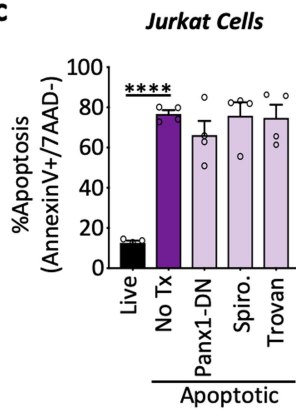
**a**



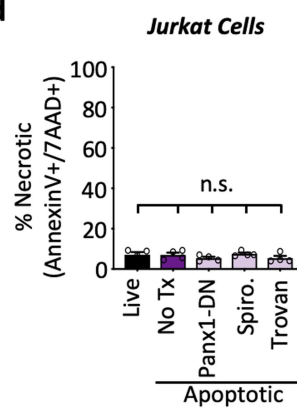
**b**



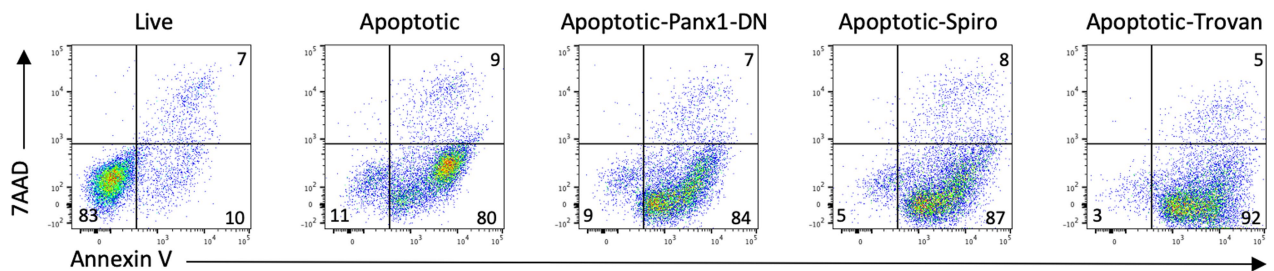
**c**



**d**

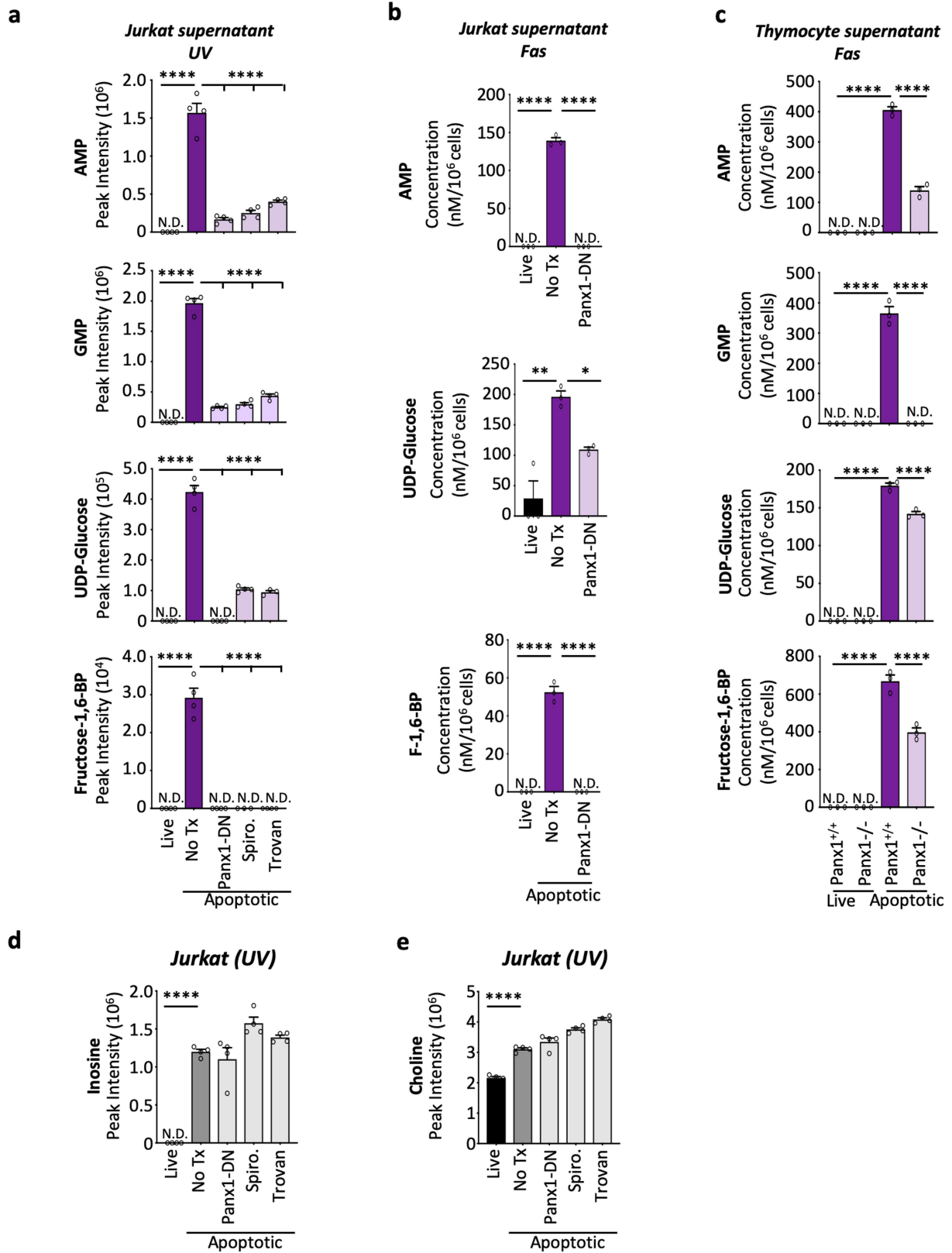


**e**



**Extended Data Fig. 5 | PANX1 inhibition does not influence apoptotic cell death.** **a**, Control (*Panx1*<sup>+/+</sup>) or *Panx1*<sup>-/-</sup> thymocytes were treated with anti-Fas antibody (5  $\mu\text{g ml}^{-1}$ ) for 1.5 h. Cells were stained with 7AAD and annexin V to determine the percentage of live, apoptotic or necrotic cells, as in Extended Data Fig. 1a. **b**, Quantification of apoptosis (top) and secondary necrosis (bottom) of control and PANX1-knockout thymocytes ( $n=3$ ). Data are

mean  $\pm$  s.e.m. \*\*\* $P=0.0004$ , ordinary one-way ANOVA with Turkey's multiple comparison test. **c**, **d**, Quantification of apoptosis (**c**) and secondary necrosis (**d**) from Jurkat cells before metabolomics analysis ( $n=4$ ). Data are mean  $\pm$  s.e.m. \*\*\*\* $P<0.0001$ , ordinary one-way ANOVA with Turkey's multiple comparison test. **e**, Cells were stained with 7AAD and annexin V to determine the percentage of live, apoptotic or necrotic cells.



Extended Data Fig. 6 | See next page for caption.

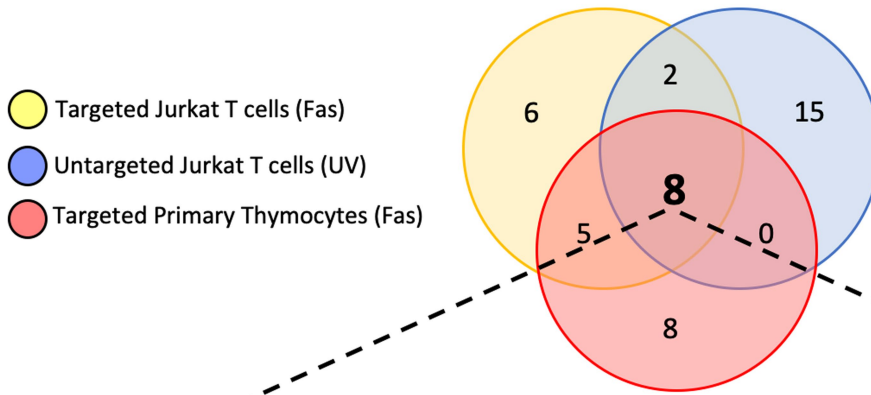
# Article

## Extended Data Fig. 6 | PAX1-dependent metabolite release during

**apoptosis. a**, Mass spectrometry was used to determine the relative amounts of AMP, GMP, UDP-glucose and FBP in supernatants from Jurkat T cells across different conditions ( $n=4$ ). Data are mean  $\pm$  s.e.m. \*\*\*\* $P < 0.0001$ , ordinary one-way ANOVA with Turkey's multiple comparison test. **b**, Jurkat cells were induced to undergo apoptosis by treatment with anti-Fas antibody ( $250 \text{ ng ml}^{-1}$ ). Mass spectrometry was used to measure the absolute concentration per million cells of AMP (top), UDP-glucose (middle) and FBP (F-1,6-BP) (bottom) in the supernatants of Jurkat T cells across different conditions (back-calculated from total cells used in experimental set-up) ( $n=3$ ). Data are mean  $\pm$  s.e.m. \* $P = 0.031$ , \*\* $P = 0.0013$ , \*\*\*\* $P < 0.0001$ , ordinary

one-way ANOVA with Turkey's multiple comparison test. **c**, Mass spectrometry was used to determine the concentrations of AMP, GMP, UDP-glucose and FBP per million cells (back-calculated from total cells used in experimental set-up) in the supernatant from isolated primary thymocytes across different conditions ( $n=3$ ). Data are mean  $\pm$  s.e.m. \*\*\*\* $P < 0.0001$ , ordinary one-way ANOVA with Turkey's multiple comparison test. **d, e**, Relative concentrations of inosine (**d**) and choline (**e**) in live, apoptotic or apoptotic supernatants in which PAX1 was inhibited were determined by mass spectrometry ( $n=4$ ). Data are mean  $\pm$  s.e.m. \*\*\*\* $P < 0.0001$ , ordinary one-way ANOVA with Turkey's multiple comparison test.

### Panx1 dependent metabolite release

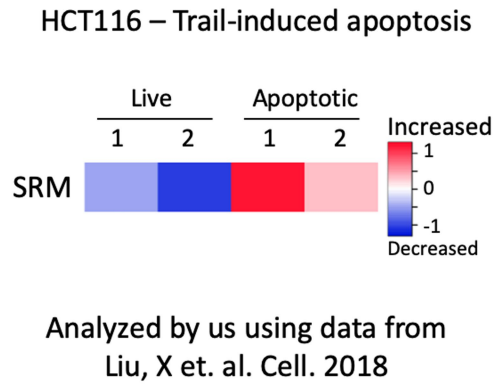


Panx1-dependent metabolites (Consistent across all platforms/conditions)	Targeted (Jurkat) (nM/10 <sup>6</sup> cells)			Untargeted (Jurkat) (Peak Intensity)			Targeted (Thymocytes) (nM/10 <sup>6</sup> cells)		
	Live	Apoptotic	Apoptotic P <sub>x</sub> 1DN	Live	Apoptotic	Apoptotic P <sub>x</sub> 1DN	Live	Apoptotic Panx1 <sup>+/+</sup>	Apoptotic Panx1 <sup>-/-</sup>
spermidine	N.D.	34	N.D.	0.3x10 <sup>6</sup>	3.0x10 <sup>6</sup>	0.8x10 <sup>6</sup>	N.D.	441	49
dihydroxyacetone phosphate (DHAP)	N.D.	3559	650	N.D.	1.2x10 <sup>6</sup>	0.2x10 <sup>6</sup>	N.D.	1471	581
Glycerol 3 - phosphate	89	697	359	0.4x10 <sup>6</sup>	5.4x10 <sup>6</sup>	1.6x10 <sup>6</sup>	42	248	166
fructose- 1,6- biphosphate	N.D.	52	N.D.	N.D.	2.9x10 <sup>4</sup>	N.D.	N.D.	668	397
adenosine 5'-monophosphate (AMP)	N.D.	139	N.D.	N.D.	1.6x10 <sup>6</sup>	0.2x10 <sup>6</sup>	N.D.	406	140
inosine 5'-monophosphate (IMP)	28	330	55	N.D.	2.2x10 <sup>6</sup>	0.09x10 <sup>6</sup>	35	140	84
guanosine 5'-monophosphate (GMP)	N.D.	208	7	N.D.	2.0x10 <sup>6</sup>	0.2x10 <sup>6</sup>	N.D.	52	N.D.
UDP-glucose	87	196	109	N.D.	4.2x10 <sup>5</sup>	2.5x10 <sup>5</sup>	N.D.	182	142

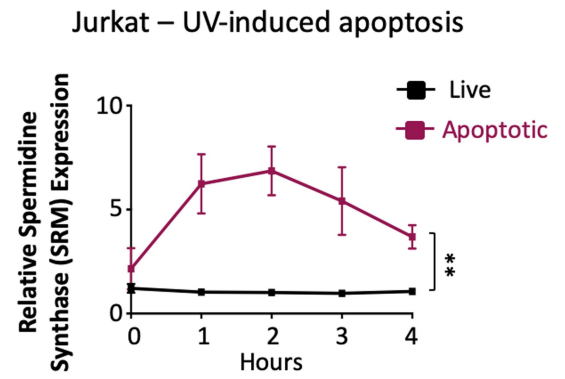
**Extended Data Fig. 7 | Conserved PANX1 secretome.** a, Top, three-way Venn diagram comparing PANX1-dependent metabolites released from apoptotic cells across different conditions tested. Bottom, table showing the relative

peak intensity (untargeted metabolomics) or absolute concentrations (targeted metabolomics) in the supernatant of the indicated cell treatments and knockout mice. N.D., not determined.

a

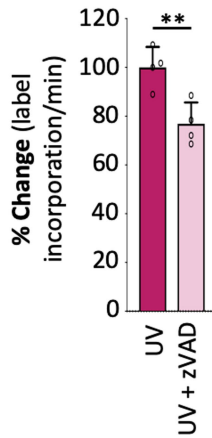


b



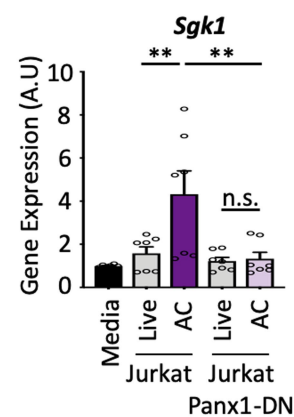
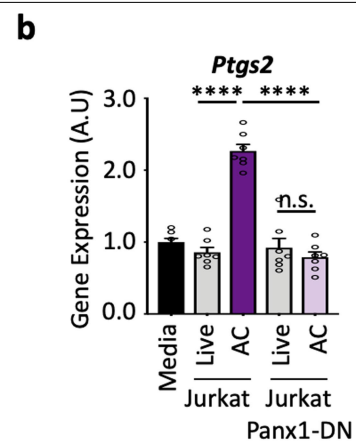
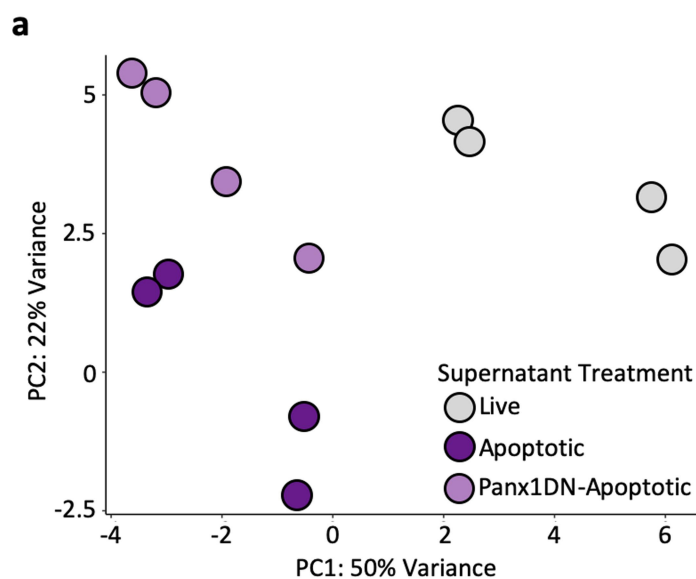
c

<sup>13</sup>C-Labeled Spermidine release (Supernatant)



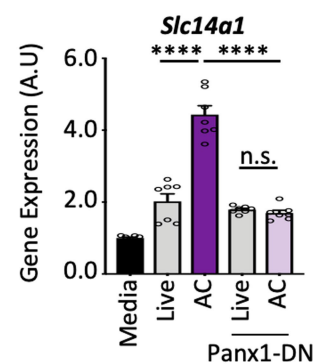
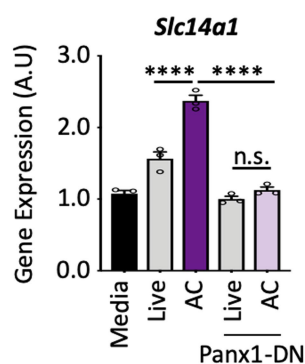
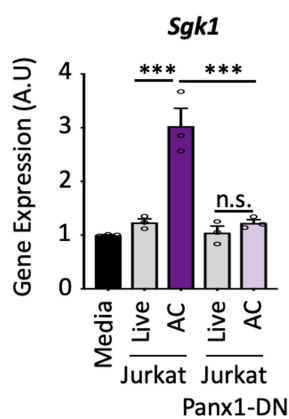
**Extended Data Fig. 8 | Transcriptional and metabolic changes during apoptosis.** **a**, Re-analyses of RNA-seq data from apoptotic cells<sup>14</sup> demonstrating that the *SRM* mRNA levels are increased or retained during apoptosis. **b**, After induction of apoptosis ( $n = 4$ ), *SRM* mRNA expression was assessed over time relative to live controls ( $n = 5$ ). Data are mean  $\pm$  s.e.m.

\*\* $P = 0.007$ , two-way ANOVA. **c**, Incorporation of <sup>13</sup>C-labelled arginine into the polyamine pathway intermediate spermidine and release from Jurkat cells after apoptosis, and its partial reduction by the pan-caspase inhibitor zVAD ( $n = 3$ ). Data are mean  $\pm$  s.d. \*\* $P = 0.0088$ , unpaired two-tailed Student's *t*-test.



**c**

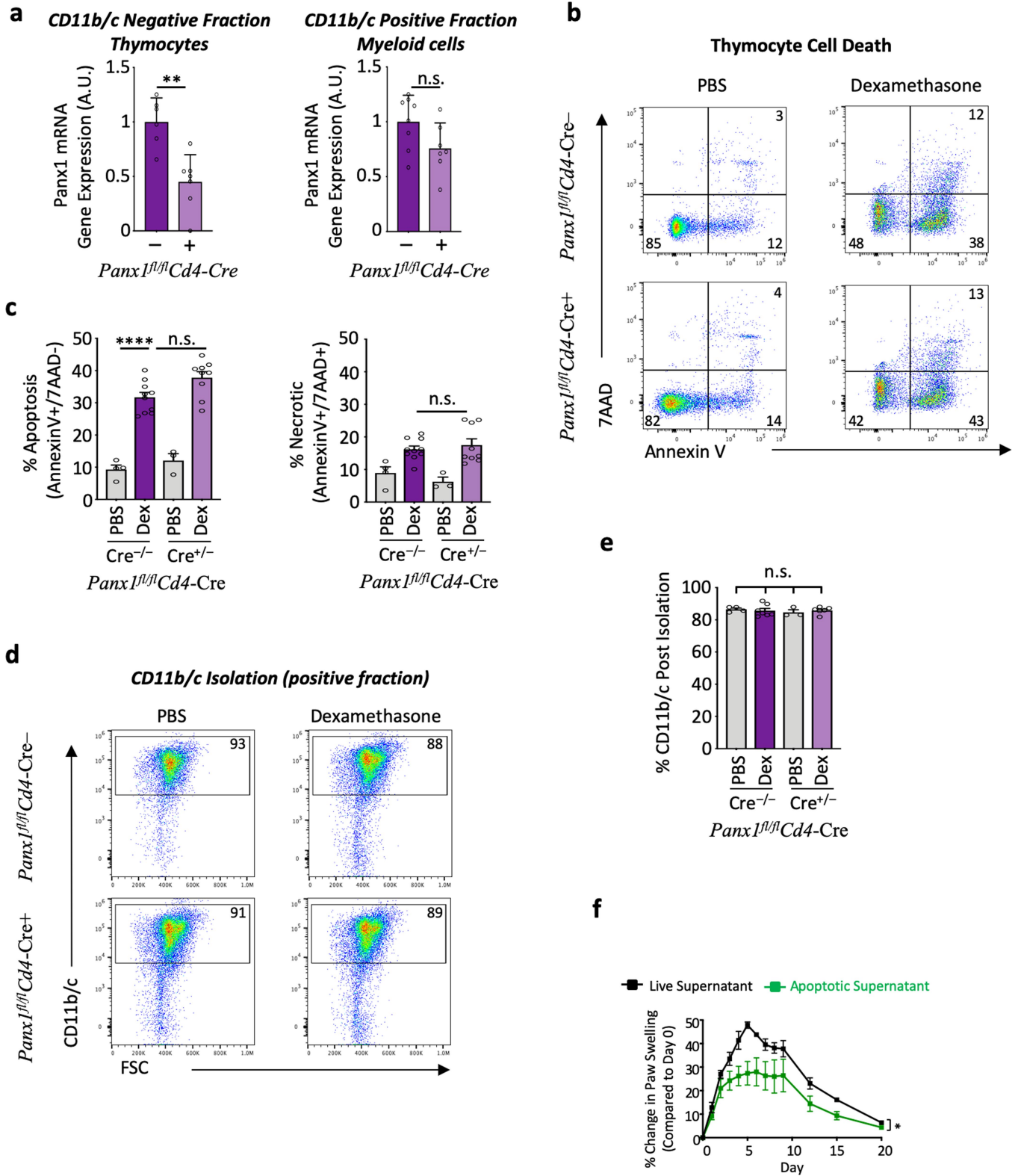
**3kDa filtered supernatant**



**Extended Data Fig. 9 | Transcriptional changes on surrounding phagocytes induced by PANX1-dependent metabolite release during apoptosis.**

**a**, Principal component (PC) analysis on the RNA-seq data as a quality control statistic ( $n = 4$  biological replicates). **b**, Experimental procedure is described in Fig. 3d. qPCR was used to assess gene expression changes in *Ptgs2* (top), *Sgk1* (middle) and *Slc14a1* (bottom) in phagocytes after treatment with supernatants from Jurkat cells or Jurkat cells expressing DN-PANX1 ( $n = 7$ ). Data are mean  $\pm$  s.e.m. Live-AC  $**P = 0.0074$  (live-AC *Sgk1*),  $**P = 0.0031$  (AC-AC

*Sgk1*),  $****P < 0.0001$ , ordinary one-way ANOVA with Turkey's multiple comparison test. **c**, Experimental procedure is as described in Fig. 3d, except before treatment of LR73 cells with supernatant, the supernatant was filtered through a 3-kDa filter to remove large molecules. qPCR was used to assess gene expression changes in *Sgk1* (top) and *Slc14a1* (bottom) in phagocytes after treatment with supernatants under specified conditions ( $n = 3$ ). Data are mean  $\pm$  s.e.m.  $****P < 0.0001$ ,  $****P < 0.0001$ , ordinary one-way ANOVA with Turkey's multiple comparison test.



Extended Data Fig. 10 | See next page for caption.

**Extended Data Fig. 10 | Analysis of thymic cell death in vivo and effects of supernatants during arthritis.** **a**, Analysis of thymic populations used for experimental data in Fig. 4a. After thymus isolation, the CD11b<sup>-</sup>CD11c<sup>-</sup> population that contained thymocytes was used for mRNA isolation to test the efficiency of deletion of the *Panx1* allele. qPCR analysis of *Panx1* mRNA in control mice (*Panx1<sup>fl/fl</sup>Cd4-cre<sup>-/-</sup>*) ( $n = 6$ ) or mice in which PANX1 has been knocked out in thymocytes (*Panx1<sup>fl/fl</sup>Cd4-cre<sup>+/-</sup>*) ( $n = 7$ ). CD11b<sup>+</sup>CD11c<sup>+</sup> myeloid cells obtained from the thymus of *Panx1<sup>fl/fl</sup>Cd4-cre<sup>+/-</sup>* mice were analysed for *Panx1* expression to demonstrate that PANX1 was not deleted. PANX1 deletion was deleted only from thymocytes and not the myeloid cells that do not express CD4. Data are mean  $\pm$  s.d.  $**P = 0.0015$ , unpaired two-tailed Student's *t*-test. **b**, Representative flow cytometric plots showing the extent of apoptosis induced by dexamethasone in control and *Panx1<sup>fl/fl</sup>CD4-Cre<sup>+</sup>* mice. After thymus isolation, cells were stained with 7AAD and annexin V to determine the percentage of live, apoptotic or necrotic cells, as in Extended Data Fig. 1a. **c**, Quantitative analysis of apoptosis (left) and secondary necrosis (right) of

CD11b<sup>-</sup>CD11c<sup>-</sup> thymic populations from *Panx1<sup>fl/fl</sup>CD4-Cre<sup>-</sup>* (PBS  $n = 4$ , Dex  $n = 10$ ) or *Panx1<sup>fl/fl</sup>CD4-Cre<sup>+</sup>* (PBS  $n = 3$ , Dex  $n = 9$ ) mice treated with PBS or dexamethasone. Data are mean  $\pm$  s.e.m.  $****P < 0.0001$ , ordinary one-way ANOVA with Turkey's multiple comparison test. **d**, Representative flow cytometry plots demonstrating the purity of CD11b<sup>+</sup>CD11c<sup>+</sup> population after magnetic separation from the different mice and treatment conditions. **e**, Comparison of the CD11b<sup>+</sup>CD11c<sup>+</sup> cells isolated under different conditions (*cre<sup>-/-</sup>*: PBS  $n = 4$ , Dex  $n = 7$ ; *cre<sup>+/-</sup>*: PBS  $n = 3$ , Dex  $n = 6$ ). Data are mean  $\pm$  s.e.m.  $P > 0.05$  (n.s.), ordinary one-way ANOVA with Turkey's multiple comparison test. **f**, Apoptotic supernatants alleviate arthritic disease induced by serum from K/Bx/N mice. C57BL/6J mice were injected with serum from K/BxN mice to induce arthritis. Live ( $n = 4$ ) or apoptotic ( $n = 5$ ) supernatant was given for five days after arthritis induction. Paw swelling was measured using a calliper and reported as the percentage change compared with day 0. Data are mean  $\pm$  s.e.m.  $*P = 0.0131$ , two-way ANOVA.

## Reporting Summary

Nature Research wishes to improve the reproducibility of the work that we publish. This form provides structure for consistency and transparency in reporting. For further information on Nature Research policies, see [Authors & Referees](#) and the [Editorial Policy Checklist](#).

### Statistics

For all statistical analyses, confirm that the following items are present in the figure legend, table legend, main text, or Methods section.

- | n/a                                 | Confirmed  |
|-------------------------------------|--|
| <input type="checkbox"/>            | <input checked="" type="checkbox"/> The exact sample size ( $n$ ) for each experimental group/condition, given as a discrete number and unit of measurement  |
| <input type="checkbox"/>            | <input checked="" type="checkbox"/> A statement on whether measurements were taken from distinct samples or whether the same sample was measured repeatedly  |
| <input type="checkbox"/>            | <input checked="" type="checkbox"/> The statistical test(s) used AND whether they are one- or two-sided<br><i>Only common tests should be described solely by name; describe more complex techniques in the Methods section.</i>   |
| <input checked="" type="checkbox"/> | <input type="checkbox"/> A description of all covariates tested  |
| <input type="checkbox"/>            | <input checked="" type="checkbox"/> A description of any assumptions or corrections, such as tests of normality and adjustment for multiple comparisons  |
| <input type="checkbox"/>            | <input checked="" type="checkbox"/> A full description of the statistical parameters including central tendency (e.g. means) or other basic estimates (e.g. regression coefficient) AND variation (e.g. standard deviation) or associated estimates of uncertainty (e.g. confidence intervals) |
| <input checked="" type="checkbox"/> | <input type="checkbox"/> For null hypothesis testing, the test statistic (e.g. $F$ , $t$ , $r$ ) with confidence intervals, effect sizes, degrees of freedom and $P$ value noted<br><i>Give <math>P</math> values as exact values whenever suitable.</i>                                       |
| <input checked="" type="checkbox"/> | <input type="checkbox"/> For Bayesian analysis, information on the choice of priors and Markov chain Monte Carlo settings  |
| <input checked="" type="checkbox"/> | <input type="checkbox"/> For hierarchical and complex designs, identification of the appropriate level for tests and full reporting of outcomes  |
| <input checked="" type="checkbox"/> | <input type="checkbox"/> Estimates of effect sizes (e.g. Cohen's $d$ , Pearson's $r$ ), indicating how they were calculated  |

*Our web collection on [statistics for biologists](#) contains articles on many of the points above.*

### Software and code

Policy information about [availability of computer code](#)

#### Data collection

Gene functions were ascribed using Uniprot and article search engines to generate a composite lists. Pathway analyses were performed using the MSigDB resource by MIT-Broad Institute. StepOne Software v2.3, BD FACSDiva V8.0, Attune NxT, StepOnePlus v2.3 and NeqSeq System Suite for the Illumina NextSeq v500, LC Q Exactive Focus (Thermo Scientific).

#### Data analysis

GraphPad Prism v.6 and v.7, SPSS v.22, R v3.3.2 (Bioconductor package DESeq2) , FlowJo v.8 and v.10 Mac, Xcalibur version 4.2.28.14 (Thermo Scientific). All code is available upon request

For manuscripts utilizing custom algorithms or software that are central to the research but not yet described in published literature, software must be made available to editors/reviewers. We strongly encourage code deposition in a community repository (e.g. GitHub). See the Nature Research [guidelines for submitting code & software](#) for further information.

### Data

Policy information about [availability of data](#)

All manuscripts must include a [data availability statement](#). This statement should provide the following information, where applicable:

- Accession codes, unique identifiers, or web links for publicly available datasets
- A list of figures that have associated raw data
- A description of any restrictions on data availability

#### Data Availability

RNA sequencing data presented in this study are in the NCBI GEO repository under the accession GSE131906.

## Field-specific reporting

Please select the one below that is the best fit for your research. If you are not sure, read the appropriate sections before making your selection.

- Life sciences     Behavioural & social sciences     Ecological, evolutionary & environmental sciences

For a reference copy of the document with all sections, see [nature.com/documents/nr-reporting-summary-flat.pdf](https://www.nature.com/documents/nr-reporting-summary-flat.pdf)

## Life sciences study design

All studies must disclose on these points even when the disclosure is negative.

Sample size	No statistical tests were used to determine sample size. For in vivo experiments, sample sizes were determined based on the numbers required to achieve statistical significance using indicated statistics.
Data exclusions	Statistical tests for outliers are routinely performed using Grubbs' test for outliers. No data was excluded in this manuscript.
Replication	Consistent results obtained from more than two technical replicates per experiment. A significant number of the experiments used at least 3-4 biological replicates.
Randomization	Allocation of mice was random in all in vivo experiments, including mice from different vivariums.
Blinding	In vivo experiments for disease models were all blinded. Researcher conducting experiments, data acquisition, data analysis, or histological scoring were blinded to treatment groups.

## Reporting for specific materials, systems and methods

We require information from authors about some types of materials, experimental systems and methods used in many studies. Here, indicate whether each material, system or method listed is relevant to your study. If you are not sure if a list item applies to your research, read the appropriate section before selecting a response.

### Materials & experimental systems

n/a	Involvement in the study
<input type="checkbox"/>	<input checked="" type="checkbox"/> Antibodies
<input type="checkbox"/>	<input checked="" type="checkbox"/> Eukaryotic cell lines
<input checked="" type="checkbox"/>	<input type="checkbox"/> Palaeontology
<input type="checkbox"/>	<input checked="" type="checkbox"/> Animals and other organisms
<input checked="" type="checkbox"/>	<input type="checkbox"/> Human research participants
<input checked="" type="checkbox"/>	<input type="checkbox"/> Clinical data

### Methods

n/a	Involvement in the study
<input checked="" type="checkbox"/>	<input type="checkbox"/> ChIP-seq
<input type="checkbox"/>	<input checked="" type="checkbox"/> Flow cytometry
<input checked="" type="checkbox"/>	<input type="checkbox"/> MRI-based neuroimaging

## Antibodies

Antibodies used	Annexin V-Pacific Blue was from BioLegend (Cat#640919, Lot#B262423). anti-CD11b-PE (clone M1/70)(Cat#12-0122-81 Lot#4278772), anti-CD11c-PE (clone N418)(Cat#12-0114-82), and anti-CD16/CD32(clone 93)(Cat#16-0161-85, Lot#4316711) were obtained from Invitrogen. Antibodies specific for Siglec-F-PE (clone E50-2440)(Cat#552126, Lot#7058859) and mouse CD95 (Cat#554254, Lot#35882) were obtained from BD. Human anti-Fas (clone CH11)(Cat#05-201, Lot#2782852) was obtained from Millipore.
Validation	All antibody lots are routinely tested by the manufacturers.

## Eukaryotic cell lines

Policy information about [cell lines](#)

Cell line source(s)	Human Jurkat Cell E6.1, HCT-116, and A549 were obtained from ATCC.
Authentication	Morphological shape of cell lines was monitored via microscopic examination.
Mycoplasma contamination	All cell lines used in the laboratory are regularly tested for mycoplasma contamination and tested negative. Additionally, all medias and serum lots used are regularly tested and tested negative.
Commonly misidentified lines (See <a href="#">ICLAC</a> register)	No commonly misidentified cell lines were used.

## Animals and other organisms

Policy information about [studies involving animals](#); [ARRIVE guidelines](#) recommended for reporting animal research

Laboratory animals	C57BL/10 and C57BL/6J wild-type mice were acquired from Jackson Laboratories. To generate mice with deletion of Panx1 in thymocytes, Panx1 <sup>fl/fl</sup> mice were crossed to Cd4-Cre mice (Taconic). KRN TCR transgenic mice were a gift from Dr. Diane Mathis at the Harvard Medical School, and were bred to NOD mice (Jackson Laboratories) to obtain the K/BxN mice. B6Nlrp1b+C11 <sup>-/-</sup> C11 <sup>-/-</sup> were a gift from Dr. Mohamed Lamkanfi's lab (VIB/UGent, Belgium). All mice used in this study were 6-12 week old. Males were used in arthritis studies and females were used for naphthalene lung model.
Wild animals	No wild animals.
Field-collected samples	No field collected samples.
Ethics oversight	Animal procedures were approved and performed according to the Institutional Animal Care and Use Committee (IACUC) at the University of Virginia.

Note that full information on the approval of the study protocol must also be provided in the manuscript.

## Flow Cytometry

### Plots

Confirm that:

- The axis labels state the marker and fluorochrome used (e.g. CD4-FITC).
- The axis scales are clearly visible. Include numbers along axes only for bottom left plot of group (a 'group' is an analysis of identical markers).
- All plots are contour plots with outliers or pseudocolor plots.
- A numerical value for number of cells or percentage (with statistics) is provided.

### Methodology

Sample preparation	Thymocytes and myeloid cells in thymus were obtained by gentle mechanical disruption. Samples were filtered prior to staining and kept on ice during staining. All fluorescent antibodies were aliquotted in a sterile hood with minimal light exposure. Staining of samples were protected from light throughout.
Instrument	Data were collected on Attune NxT (Invitrogen).
Software	Data were analyzed using FlowJo V10 Software.
Cell population abundance	Purity of isolated samples was obtained by antibody stain and FACS. Sample purity was greater than 90%.
Gating strategy	Standard lymphocyte gates were applied, following by doublet exclusion using FSCHxW and SSC-HxW. Myeloid cells in thymus were gated using CD11b and CD11c. Apoptosis of cells were gated using Annexin V and 7AAD. Pannexin-1 activation was measured using TO-PRO-3 dye. Representative Flow plots are shown are in Figures and Extended Data.

- Tick this box to confirm that a figure exemplifying the gating strategy is provided in the Supplementary Information.